DETERMINATION OF SUSCEPTIBILITY TO INTERGRANULAR CORROSION IN AISI 304L AND 316L TYPE STAINLESS STEELS BY ELECTROCHEMICAL REACTIVATION METHOD

A THESIS SUBMITTED TO
THE GRADUATE SCHOOL OF NATURAL AND APPLIED SCIENCES
OF
MIDDLE EAST TECHNICAL UNIVERSITY

BY

GÜLGÜN HAMİDE AYDOĞDU

IN PARTIAL FULFILLMENT OF THE REQUIREMENTS
FOR
THE DEGREE OF MASTER OF SCIENCE
IN
METALLURGICAL AND MATERIALS ENGINEERING

DECEMBER 2004

Approval of the Graduate School of Natural and Applied Sciences

_____

Prof. Dr. Canan ÖZGEN
Director

I certify that this thesis satisfies all the requirements as a thesis for the degree of Master of Science.

_____

Prof. Dr. Tayfur ÖZTÜRK
Head of Department

This is to certify that we have read this thesis and that in our opinion it is fully adequate, in scope and quality, as a thesis for the degree of Master of Science.

_____

Assoc. Prof. Dr. M. Kadri AYDINOL
Supervisor

Examining Committee Members

Prof. Dr. Mustafa DORUK (METU, METE) _____

Assoc. Prof. Dr. M. Kadri AYDINOL (METU,METE) _____

Prof. Dr. Şakir BOR (METU, METE) _____

Prof. Dr. Tayfur ÖZTÜRK (METU,METE) _____

Dr. Alp ALANYALIOĞLU (KALEBOZAN) _____

I hereby declare that all information in this document has been obtained and presented in accordance with academic rules and ethical conduct. I also declare that, as required by these rules and conduct, I have fully cited and referenced all material and results that are not original to this work.

Name, Last name : Gülgün H. Aydoğdu

Signature :

ABSTRACT

DETERMINATION OF SUSCEPTIBILITY TO INTERGRANULAR CORROSION IN AISI 304L AND 316L TYPE STAINLESS STEELS BY ELECTROCHEMICAL REACTIVATION METHOD

Aydoğdu, Gülgün Hamide
M.S., Department of Metallurgical & Materials Engineering
Supervisor: Assoc. Prof. Dr. M. Kadri Aydınol

December 2004, 75 pages

Austenitic stainless steels have a major problem during solution annealing or welding in the temperature range of 500-800 °C due to the formation of chromium carbide, which causes chromium depleted areas along grain boundaries. This means that the structure has become sensitized to intergranular corrosion. Susceptibility to intergranular corrosion can be determined by means of destructive acid tests or by nondestructive electrochemical potentiokinetic reactivation (EPR) tests. The EPR test, which provides quantitative measurements, can be practiced as single loop or double loop. Single loop EPR method for AISI 304 and 304L type stainless steels was standardized; however double loop EPR (DLEPR) method has not been validated yet.

In this study, the degree of sensitization was examined in AISI 304L and 316L type steels by DLEPR method whose experiments have been carried out on sensitive and nonsensitive steels to examine and

determine the detailed parameters; solution temperature, concentration and scan rate of the DLEPR method.

In order to determine the degree of sensitization, oxalic acid, Huey and Streicher tests were carried out and revealed microstructures and measurements of weight loss by the acid tests were then correlated with DLEPR method results, as a first step towards standardization of DLEPR method for 316L steels. Best agreement was provided with test parameters which are 1M H_2SO_4 + 0.005M KSCN at 3 V/hr scan rate with 30 °C solution temperature. It was concluded that specimens can be classified as step, dual and ditch, if the I_r:I_a ratios were obtained to be between 0 to 0.15, 0.15 to 4.0 and 4.0 to higher respectively.

Key words: Intergranular corrosion, DLEPR test method, austenitic stainless steel.

ÖZ

AISI 304L VE 316L TİPİ PASLANMAZ ÇELİKLERİN TANELER ARASI KOROZYONA DUYARLILIĞININ ELEKTROKİMYASAL REAKTİVASYON YÖNTEMİYLE BELİRLENMESİ

Aydoğdu, Gülgün Hamide
M.S., Metalurji ve Malzeme Mühendisliği Bölümü
Tez Yöneticisi: Doç. Dr. M. Kadri Aydınol

Aralık 2004, 75 sayfa

Tavlama veya kaynak işlemleri sırasında, 500-800 °C sıcaklık aralığında, tane sınırları boyunca kromca azalan bölgelere sebep olan krom karbürün oluşumundan dolayı östenitik paslanmaz çelikler önemli bir sorun yaşanabilir. Taneleraras korozyona duyarlılık, yıkıcı olan asit testleri ya da yıkıcı olmayan elektrokimyasal potansiyokinetik reaktivasyon (EPR) testleri tarafından belirlenebilir. Nicel ölçümler sağlayan EPR testi tek veya çift çevirimli olarak uygulanabilir. Tek çevirimli EPR test metodu 304 ve 304L tipi paslanmaz çeliklerde standartlaştırılmış, fakat çift çevirimli EPR (DLEPR) metodunun henüz geçerliliği sağlanmamıştır.

Bu çalışmada, AISI 304L ve 316L tipi östenitik paslanmaz çeliklerde, taneleraras korozyona duyarlılığın derecesi DLEPR metodu ile incelendi. Bu test metodunun parametreleri, (tarama hızı, çözelti konsantrasyonu ve sıcaklığı gibi) duyarlı ve duyarlı olmayan paslanmaz çelikler üzerinde deneyler yapılarak belirlendi.

Tanelerarası korozyona duyarlılığın derecesinin belirlenmesi için Oxalic asit test, Huey and Steicher test metodları uygulandı. 316L tipi paslanmaz çeliklerin DLEPR metodu kullanarak tanelerarası korozyona duyarlılığını belirleme yönünde bir ilk adım olarak, asit test metodu aracılığıyla sonuçlanan mikroyapılar ve ağırlık kayıp ölçümleriyle DLEPR metodunun sonuçları arasında ilişki kuruldu. En iyi uyum 1M H_2SO_4 + 0.005M KSCN test solusyonu, 3 V/hr tarama hızı ve 30 °C solusyon sıcaklığı ile sağlanmıştır. Eğer I_r:I_a akım oran değerleri, 0-0.15, 0.15-4.0 ve 4.0 ve daha yükseği olarak belirlenmişse, numunelerin sırasıyla step, dual ve ditch yapı olarak sınıflandırılabileceği sonucuna varılmıştır.

Anahtar kelimeler: Tanelerarası korozyon, DLEPR test metodu, östenitik paslanmaz çelik.

To My Yener

ACKNOWLEDGEMENTS

I would like to thank first my supervisor, Assoc. Prof. Mehmet Kadri Aydınol. Throughout my thesis-writing period, I would not have been even able to finish this project without his enthusiasm, his inspiration, his help with experimental setup and his great efforts to explain things clearly and simply.

I would like to thank sincerely Prof. Dr. Mustafa Doruk. He provided an occasion on studying of this subject and encouragement, precious advice, good teaching from the beginning to end of the study.

I am also grateful to especially Tufan Güngören, Elif Tarhan, Ziya Esen, Gül Çevik, Melih Topçuoğlu, Fatih Şen Gürçağ for their support and help, when it was most required.

I am forever grateful to my husband Yener Kuru and my parents Ekrem-Güner Aydoğdu, my grandmother Hamide Taşan, my sister Nilgün Aydoğdu, her husband Armağan Barut and my friends Pınar, Hande, Başak, Gülsen, Burcu for their endless understanding, patience and encouragement throughout my life.

Finally, I would like to thank the technical staff of Middle East Technical University, Department of Metallurgical and Materials Engineering especially Res. Assoc. Cengiz Tan and Erdinç Cıstık for making things a lot easier.

TABLE OF CONTENTS

CHAPTER I

INTRODUCTION

Man encounters with corrosion into many parts of our lives due to its significant harm. The word corrosion denotes the destructive result of chemical or electrochemical reactions between a metal or metal alloy and its surroundings. The nature of this reaction depends not only on the chemistry of the system but also the structure of the metal. For example, grain boundaries, which are imperfect and high energy regions, generally weaken the corrosion resistance of materials due to the depletion of corrosion resistance alloying elements on the grain boundaries.

The best known example of metallurgical effect on corrosion is intergranular corrosion which is mostly observed on the use of austenitic stainless steels. Austenitic stainless steels (containing 18% Cr - 8% Ni) are widely used in steam generating plants as piping and superheating tube materials due to their good mechanical properties and corrosion resistance at elevated temperatures. However, when austenitic stainless steels have undergone a treatment like welding in the temperature range between 500 - 800 °C, there is a breaking corrosion resistance intergranularly as a result of segregation of chromium carbides, that is, it has become sensitized. High concentration of chromium in $M_{23}C_6$ particles decreases locally the chromium content in the region that is adjacent to these Cr rich precipitates.

In austenitic stainless steels, corrosion resistance is provided by a very thin surface film, known as passive film that is an invisible film of oxide, formed by the metal reacting with the ambient environment. Normally these films are free of pores, but their stability may be weakened locally. It therefore has different properties in areas where the steel surface is altered

due to grain boundary precipitates. This heterogeneous microstructure is very dangerous since it weakens steel without much change in the outward appearance.

There are several test methods, which have been used for determining this sensitization. Acid immersion test was firstly standardized and testing procedure was presented in ASTM A 262-91 [1]. Corrosion rate is determined by weight loss and classification of structure in many highly oxidizing media. Another proposed way of measuring the degree of sensitization to intergranular corrosion involves electrochemical reactivation of the sample. This reactivation process is named as electrochemical potentiokinetic reactivation (EPR) and has been developed in single loop (SLEPR) [2] or in double loop (DLEPR) types.

In this study, DLEPR was applied for the determination of susceptibility to sensitization in 304L and 316L type stainless steel. The objective is to examine the effects of parameters in the double loop test method and determine the optimum conditions to obtain reliable and quantitative results. These parameters can be solution temperature, composition and scan rate. In this respect, the effects of sulfuric acid (H_2SO_4), potassium thiocyanate (KSCN), potassium chloride (KCl) additions and their concentrations on the activation and the reactivation behavior of AISI 304L type stainless steels were investigated. The usual outcome of the DLEPR test used in determining the susceptibility of the steel are the anodic and reverse scan currents. Therefore current and also in this study charge per cm^2 of the specimen surface were monitored. A similar procedure was applied for the determination of the test parameters to give the optimum result that should be used for the evaluation of sensitization of AISI 316L stainless steels which was then compared with the results of acid tests.

CHAPTER II

LITERATURE SURVEY

II.1. Austenitic Stainless Steels and Intergranular Corrosion

Stainless steels, which are used as corrosion-resistant equipments in most major industries like architectural, automobile, food and chemical industries, are iron alloys containing chromium. There are three main classes of stainless steel designated in accord with their metallurgical structure; austenitic (face centered cubic), ferritic (body centered cubic) and martensitic (body centered tetragonal or cubic). In austenitic class, it is named due to austenite phase, which exists as a stable structure between 910 °C and 1400 °C for pure iron and is the only matrix phase at room temperature, existing as a stable or metastable structure depending on composition. The stability of the austenite phase at low temperatures is achieved with the addition of nickel. In the common alloy, the atomic arrangement would be expected about one in five of the atoms being chromium and about one in thirteen being nickel, a substitutional solid solution of chromium and nickel in iron. In addition, when the addition of a ferrite stabilizer like molybdenum, nickel content of steel must be increased at the same time to maintain the austenitic structure. Atoms of other elements are also present; carbon is distributed in the interatomic spaces, but may form carbides according to the prior history of alloy.

The austenitic stainless steels, which are non magnetic, are designated by the AISI with the numbers in 200 and 300 series. Some of the more common 300 series austenitic stainless steels are identified as types

AISI 304 and AISI 316. Type 304L and 316L are a lower carbon modifications and type 316 contains approximately 2% molybdenum.

Corrosion resisting properties of Fe-Cr-Ni alloys are influenced by chromium than by any other alloying element that may be present. Chromium itself is chemically more reactive element than iron. The high degree of reactivity of chromium is actually the principal basis for corrosion resistance. The effect of chromium in corrosion resistance to iron under favorable conditions is the formation of protective film, which is formed by the reaction between chromium and oxygen. Under reducing conditions corrosion resistance is provided by this film.

Nickel is less reactive than either iron or chromium. At the same time, nickel, like chromium but to a lesser extent, has the property of being able to protect itself with a passive oxide film and to contribute this property to other metals with nickel alloyed. The most common alloy of this type contains about 18% Cr and 8% Ni. Moreover, local corrosion or pitting tends to progress less rapidly in Ni containing alloys. Therefore, other than the effect of stabilizing austenite, the effect of nickel in these alloys is also some corrosion resistance in both oxidizing and reducing solutions [3].

Molybdenum is used in Fe-Cr-Ni alloys most commonly in the range from 2 - 4 weight percentage which has strong effects in improving the resistance of these alloys to chemical attack, particularly in certain organic acids, dilute solutions of sulfuric acid and in chloride solutions [3]. Molybdenum seems to decrease the break down of oxide films under reducing conditions. In addition, the presence of the molybdenum which decreases the probability of pit formation improves the stability of the passive film.

Figure II-1 [4] shows the phase relationships in an alloy of composition 18% Cr, 8% Ni and 74% Fe. As it is seen, the carbon solubility in austenite decreases with decreasing temperature. Quenching from the austenite region causes carbon to stay in the solid solution. This supersaturated carbon will than precipitate as carbides ($M_{23}C_6$), if the alloy is reheated to a temperature below the solubility limit. High concentration of chromium in $M_{23}C_6$ particles

(metal atom content of carbide may include Fe, Mo and Cr) decreases locally the chromium content in the regions that are adjacent to these chromium rich precipitates. Carbon is a small atom and diffuses much more fast. However chromium can not find enough time to gather and to form the carbide, therefore it requires a fast diffusion path like high angle grain boundaries. Thus, while the carbon atoms migrate to the grain boundary from all parts of the crystal, chromium is depleted from more localized regions near the grain boundary.

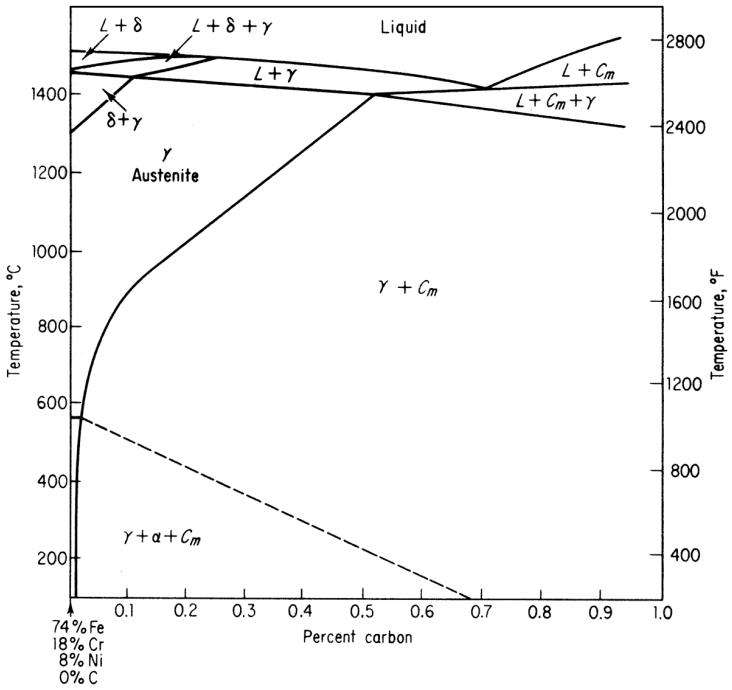

Figure II-1. Phase diagram for 74%Fe-18%Cr-8%Ni alloy [4].

In the region that is near grain boundaries, as it is seen from Figure II-2 [5], chromium content lowers to below 13%, which is a critical value for required stainless corrosion behavior. Because of chromium depletion along grain boundaries, the corrosion resistance is broken down and it proceeds

intergranularly. The austenitic stainless steel in which chromium carbides have precipitated on grain boundaries is said to be sensitized and is susceptible to intergranular corrosion. However, it is understood from the Figure II-2 that at prolonged treatments, chromium diffusion from the bulk of the grain increases the concentration above the critical limit and heals the boundaries.

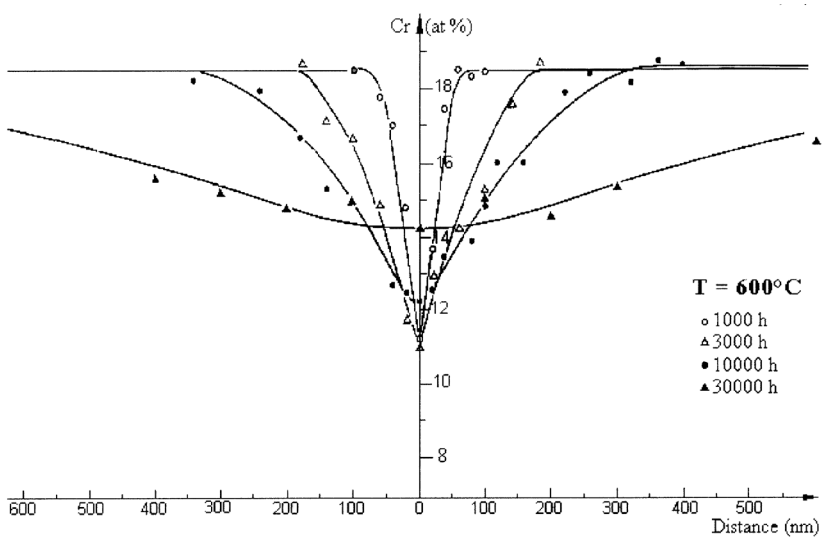

Figure II-2. Chromium concentration profile of 316L type stainless steel across a grain boundary during ageing at 600 °C [5].

The diffusion of chromium atoms below 500 °C, required for $M_{23}C_6$ formation, is too sluggish even at grain boundaries that carbide formation essentially stops. Above 800 - 900 °C, however, chromium and carbon are dissolved as atoms in the crystal structure of austenite and there is no thermodynamic driving force for chromium carbide formation. In order to check susceptibility of stainless steels, half an hour at 650 °C is usually regarded as sensitizing treatment for 18/8 Cr-Ni steels [6], but sensitizing time can be prolonged according to steel composition.

The results of intergranular corrosion have led to remedy this problem with eliminating or reducing the formation of $M_{23}C_6$ carbides. One way is to select an extra-low carbon modification of 304 and 316, which are 304L and 316L (upper limit of carbon is 0.03%). A decrease in carbon content from 0.08 - 0.02 wt% C, the nose of the carbide curve on precipitation kinetics of $M_{23}C_6$ is shifted from 0.1 hr to 100 hr [7, 8]. It can be understood that although chromium carbide formation may not completely suppressed, it can be greatly delayed by this way.

Second way is the solution treatment, which dissolves $M_{23}C_6$ carbides and the following rapid cooling, prevents re-precipitation of carbides in the critical temperature range. Third one is the addition of strong carbide formers like titanium and niobium. These carbide stabilizing elements react with carbon at higher temperatures to precipitate the carbide so that little carbon is left to precipitate as chromium-rich grain boundary carbide during cooling.

Another way in controlling the $M_{23}C_6$ carbide formation kinetics, is the addition of molybdenum to Cr-Ni stainless steels, which markedly lengthens the sensitization time [9]. Sensitization heat treatment for 316 and 316L type stainless steels requires much longer holding times at the critical temperature range compared to 304 and 304L respectively. According to AISI standards for 316L, the added molybdenum was taken from chromium and in order to suppress the ferrite stabilization effect of molybdenum, nickel content is increased. Increased nickel decreases the solubility of $M_{23}C_6$ carbide in austenite [8]. Similarly, increasing molybdenum content also lowers the solubility of $M_{23}C_6$ carbide in austenite. Molybdenum dissolves in carbide [8], renders it more stable and accelerates its formation. However, lower chromium causes an increase in the solubility of carbon in austenite, which decreases the kinetics of $M_{23}C_6$ carbides [7]. In addition, there is a slight drop in the chromium content of the $M_{23}C_6$ carbide in 316 and 316L type stainless steels due to the Mo enrichment of the carbide [10]. The most important effect of molybdenum addition, however is on the diffusivities of both chromium and carbon in austenite. At 650 °C, chromium diffusivities are about $1x10^{-15}$ and $2x10^{-16}$ cm/s, while carbon diffusivities are about $2x10^{-5}$

and $6x10^{-6}$ cm/s for types 304 and 316 respectively [11]. As it is seen there is a marked slowing down of diffusion kinetics. In the overall, sensitization treatment for 316 and 316L type steels lengthens. One more important consequence of carbide formation along grain boundaries in molybdenum containing stainless steels, is the depletion of molybdenum as well [10, 12].

The exposure of austenitic stainless steel to elevated temperatures for long periods of time can result in formation of various other phases. In Figure II-3 [13], a time-temperature-precipitation (TTP) diagram for type 316 and 316L type stainless steel is shown. It is clear from this figure that the precipitation of $M_{23}C_6$ carbide can occur in short times, however precipitations of the other phases (sigma, chi, laves phases) require longer time and/or higher temperatures. In 316 type, with its increased carbon content, formation of intermetallic phases are realized in time periods 10 times longer than 316L. However carbide formation is started at minutes level in 316, compared to hours level in low carbon 316L.

The formation of the intermetallic phases, which is delayed due to the slower diffusion of substitutional elements required for their nucleation and growth, results in a depletion of chromium and molybdenum in austenite matrix [14, 15]. This causes a detrimental effect on the corrosion resistance, especially pitting, intergranular and crevice corrosion. Sigma (σ) phase with formula FeCr, which is more generally expanded as $(FeNi)_x(CrMo)_y$, is a severe problem due to its effect on the mechanical properties and localized corrosion resistance [16]. It nucleates mainly on the grain boundaries and is found in 316L type stainless steels approximately in 100 hours at 800 °C. Laves (η) phase (Fe_2Mo) formation is observed after a minimum 10 hour at 750 °C predominantly on dislocations. Chi (χ) phase with composition $Fe_{36}Cr_{12}Mo_{10}$ is a minor intermetallic phase and found at 800 °C for 10 hour.

In 304 type stainless steels, only sigma phase formation occurs. In 304 type steel containing 0.05% C, its formation was observed in few thousand hours at 750 °C [15].

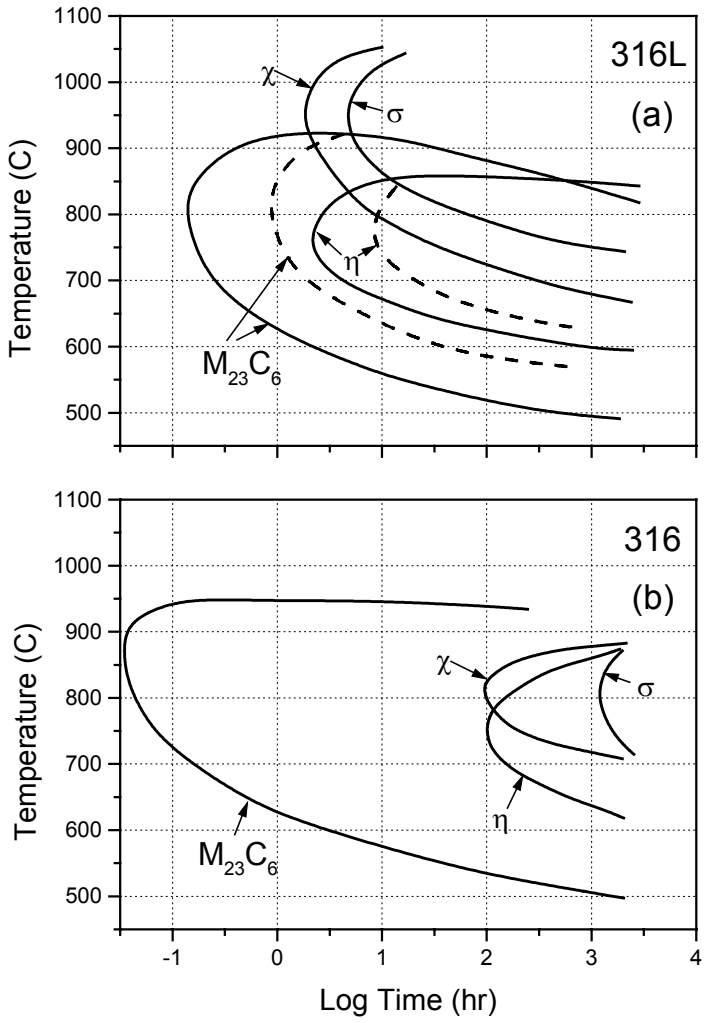

Figure II-3. Time-temperature-precipitation diagram of (a) type 316L and (b) type 316 [13]. Dashed curves are for steels solution treated at 1090 °C for 1 hr and solid curves are for steels solution treated at 1260 °C for 1.5 hr.

II.2. Electrochemical Nature of Corrosion on Metals

Natural tendency of the metal is to combine with environmental elements and to revert to a lower energy state. This decrease of energy is the driving force of the corrosion reactions. These reactions involve electron or charge transfer in aqueous solutions. The free energy change determines

the spontaneity of all reactions. It is mathematically related to electromotive force (EMF), which is calculated from Nernst equation. Most metals are reactive in an oxidizing environment. Metal dissolution starts when the Nernst equilibrium potential is exceeded. Potential/pH diagrams, which are considered by Marcel Pourbaix, are as a map showing relations of potential and aqueous solution, derived from Nernst equation.

Moreover, reactive metal surface is protected by the formation of passive surface layers in oxidizing environments. The resistance of metals and alloys to chemical effects of active corrosives is generally determined by the ability of the materials to protect themselves through the formation of poreless, thin, continuous, insoluble films. The formation of these oxide films causes a characteristic polarization curve of metals.

II.2.1. Anodic Polarization

The corrosion process consists of a set of redox reactions, which are electrochemical in nature. The metal is oxidized to corrosion products at anodic sites and general oxidation reaction is $M \rightarrow M^{+n} + ne^{-}$. This removes the metal atom by oxidizing it to its ion. All electrons generated by the anodic reactions are consumed by corresponding reduction reactions at cathodic sites of a corroding metal or at the cathode of an electrochemical cell. For example, one of the cathodic reactions is the reduction of hydrogen ions, $2H^{+} + 2e^{-} \rightarrow H_2$.

The anodic and cathodic reactions are controlled by the flow of the electrons through the metal. The transfer of electrons in these reactions is the corrosion current. As current flows, the anodic and cathodic potentials are displaced from the equilibrium or reversible values and approach each other. This process is called polarization. The polarization measurements are made with potentiostat which maintains the desired potential between the electrode being studied (working electrode) and reference electrode by passing the current between working and inert counter electrode. In a polarization diagram the first measurements is the corrosion potential when the applied

current (i_{appl}) is zero. When total rates of anodic reactions are equal to the total rates of cathodic reactions, corrosion potential is called open circuit potential (E_{corr}), seen in Figure II-4. The current density at E_{corr} is called the corrosion current density (i_{corr}).

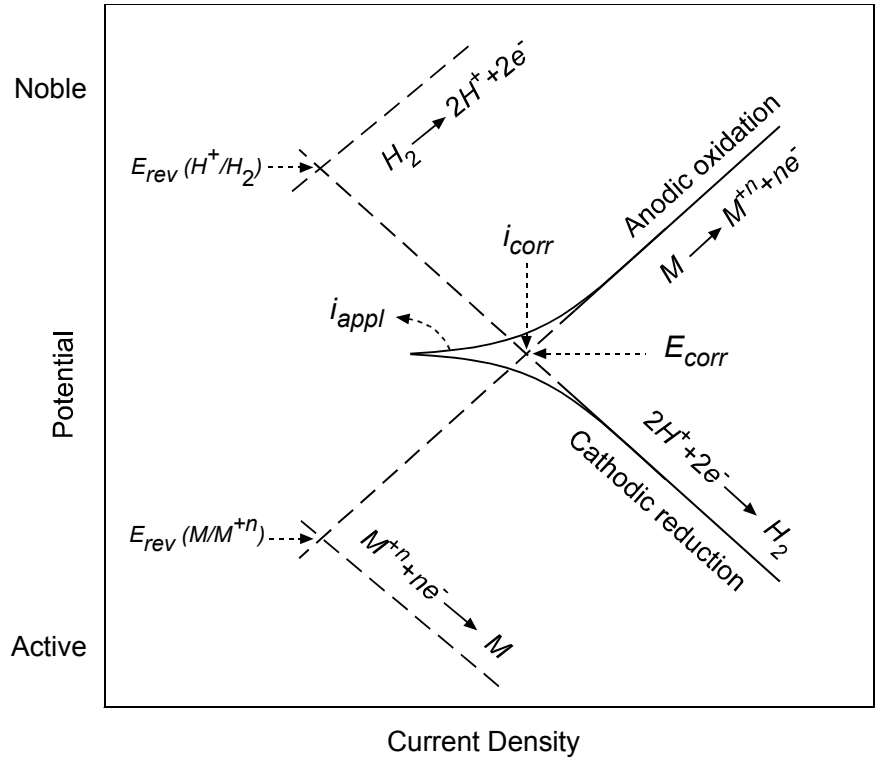

Figure II-4. Corrosion potential and current density.

When the applied potential is increased to more positive value (noble) than the specimen open circuit potential (E_{corr}), the specimen behaves as anodic and metal dissolution reaction is realized, see Figure II-5. This is represented as anodic polarization curve. Anodic current density is

proportional to the corrosion rate of metal. If the potential is increased, the rate of corrosion rises rapidly. This the active range of the metal. If the potential is raised further, the corrosion will drop suddenly to a lower value, then it will remain constant over a wide potential range. This is the passive range, in which a thin, invisible film of oxide covers the metal. This protective film acts as a barrier between the metal and its environment and reduces its rate of dissolution. If the potential is kept on increasing, corrosion rate will rise again, since the passive film will be dissolved. This is called the transpassive range.

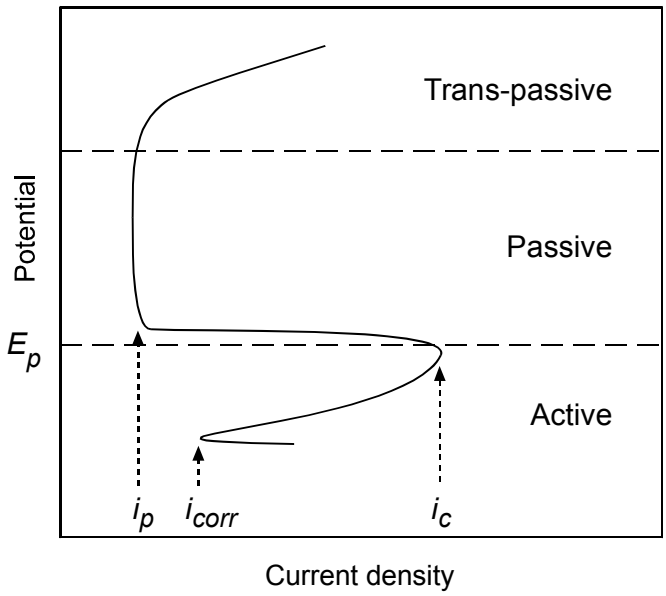

Figure II-5. Schematic anodic polarization curve.

The critical values on the anodic polarization curve are affected by the temperature and pH of medium. At higher temperatures and lower pH, critical current density (i_c) increases. It means the transport to passive range can be

realized difficultly. The passivation potential (E_p) and passivation current density (i_p) increase slightly as well [17].

Polarization curves changes from metal to metal depending on how the metal can easily be passivated. It can be seen in the Figure II-6 [18] that chromium is easily passivated since its passivation potential (E_p) and critical current density (i_c) are lower. Also, chromium is passive over a broad range. However, iron has a higher critical current density and passivation potential. For nickel, anodic current changes continuously in the passive range and increases with a peak to transpassive range.

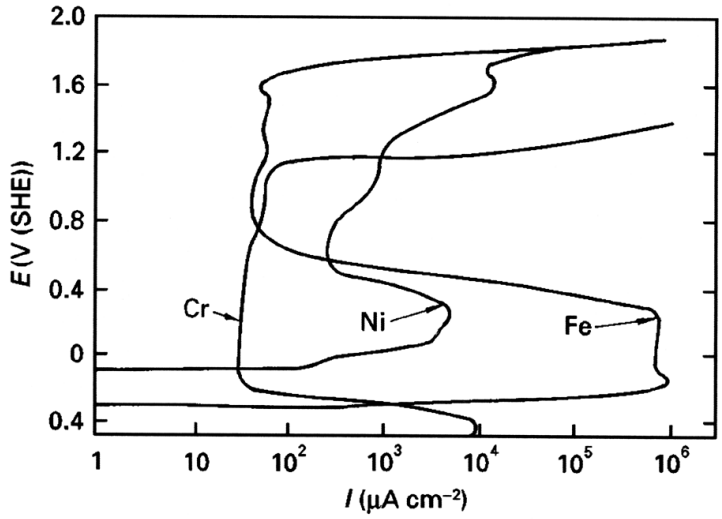

Figure II-6. Anodic polarization diagram of pure Cr, Ni and Fe in 1N H_2SO_4 [18].

As it is seen in Figure II-7 [19], molybdenum also contributes to passivity. Its polarization behavior is different compared to Fe and Ni. Anodic current density of molybdenum does not increase steeply with the potential [19]. On the other hand, if corrosion potential is observed, the corrosion potential of Fe18Cr14.3Ni2.5Mo alloy is more noble than Cr and Fe but close to that of Ni and Mo and this is typical for austenitic alloys. As a

consequence, it is shown that Ni and Mo are enriched on the surface in the metallic state during anodic polarization [20].

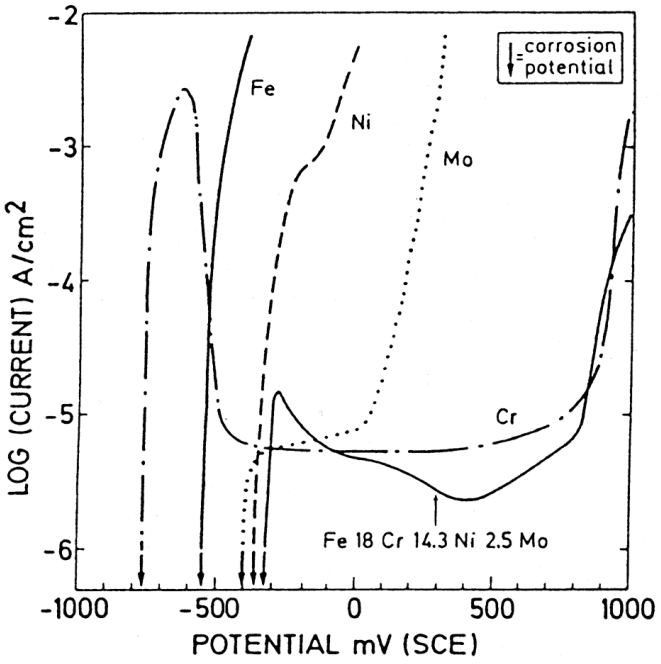

Figure II-7. Anodic polarization curves of pure metals, Fe, Ni, Cr, Mo and Fe18Cr14.3Ni2.5Mo (at%) austenitic stainless steel in 0.1M HCl + 0.4M NaCl at 25 °C and 3mV/s [19].

Alloying the steel with both chromium and nickel accelerates the passivation. Even, addition of small amounts of molybdenum to Cr-Ni steels reduces the critical current density and also Mo alloyed steel is passive in broad potential range. Molybdenum also improves the pitting resistance of the steel especially in chloride environments. In solutions containing halogen ions, like chloride, polarization curve changes considerably. For example, passivation is realized more difficultly and the stability of passivation cannot be maintained, which is because of the aggressive attack of the chloride ion. In molybdenum containing stainless steels, it should be understood that, the

formation of sigma and chi phases decreases the passive potential range because of chromium and molybdenum depletion in the matrix [21].

II.2.2. Passivity

Passivity is not an absolute property of a material like melting point. A metal has variable degrees of passivity, which is measured by potential, reaction and corrosion rate. Uhlig defines passivity by two closely linked definitions [22]:

> "*1. A metal is passive if it substantially resists corrosion in a given environment resulting from marked anodic polarization.*
> *2. A metal is passive if it substantially resists corrosion in a given environment despite a marked thermodynamic tendency to react*."

It means that oxidizing conditions favor passivity while reducing conditions destroy it, or anodic polarization passivates but cathodic polarization activates. For example, iron in contact with a more noble metal (corresponding to anodic polarization) is passivated whereas with a less noble metal, passivity is difficult to attain.

For explaining the nature of the passive film, there are mainly two theories of passivity, which are oxide film theory and adsorption, or electron configuration theory.

According to electron configuration theory, in stainless steels, iron can be transformed to passive state by sharing electron with chromium, which has stronger tendency to adsorb electron. Chromium with 5 vacancies in the *3d* shell of the atom can share at least 5 electrons or can passivate 5 iron atoms. This proportion corresponds to 15.7 wt % chromium. That is, stainless Cr-Fe alloys are produced at critical minimum amount of chromium about 12% [23].

According to oxide film theory, a diffusion barrier layer of reaction products, which are metal oxide or other compounds, separates metal from

its environment and slows down the rate of reaction. Its thickness and composition can change with alloy composition, electrolyte and potential. The passive film of austenitic stainless steel is presented as duplex layer, which consists an inner barrier oxide film and outer hydroxide film [20, 24].

Main compounds in the passive film on Fe-Cr alloy are oxide products of Cr, although iron oxides generally predominate. The passive potential range consists of Fe^{+3}, Cr^{+3} and Fe^{+2}. Fe^{+3} oxide is reduced to Fe^{+2} hydroxide and finally to Fe metal. Cr stops the reduction of iron to metallic state and Cr^{+3} is not reduced, remains within the passive layer [25].

Nickel is oxidized only to a very low extent. Its positive influence is not in passive film, but in the underlying metal phase, it provokes passivibility of the alloy [26]. On the other hand, with molybdenum addition the passivity of stainless steel is improved and oxide product is enriched. Also, molybdenum in the alloy redissolves into solution and forms molybdenate ion, which adheres the surface to prevent the attack of chloride ions [26, 27].

Intergranular corrosion on Fe-Cr-Ni alloys is due to local deterioration of passive film. Thus, passive state of sensitive stainless steel is less stable than that of non-sensitive steel [28].

II.3. Techniques for Measuring Susceptibility to Intergranular Corrosion

Studies of the conditions for intergranular corrosion and its mechanism have been the subject of numerous investigations. Determination of how sensitive the steel to intergranular attack is therefore of prime importance. Various evaluation tests have been developed to determine the susceptibility of austenitic stainless steel to intergranular attack. For long time, before the electrochemical techniques were developed, and acid immersion tests have been used.

Acid tests have simple principles that consist in subjecting the steel under examination to contact with a test medium. The purpose of the test medium is to attack the Cr-depleted zone in steel containing grain boundary

carbide. Evaluation of corrosion rate is provided comparatively by visual, microscopic examinations and weight loss of the steel.

Intergranular attack is accelerated by potential differences between grain and grain boundaries, that is, attack is determined by availability of anodic sites at grain boundaries. Therefore, making it anodic passivates the specimen. At that time, the chromium depleted alloy sets up passive-active cell of appreciable potential difference, the grains (exhibit passive behavior) constituting large cathodic areas relative to small anode areas at grain boundaries (exhibit active behavior). During decreasing the potential, the protective passive film over Cr-depleted areas is more easily dissolved than that over undepleted (non-sensitized) surfaces. The electrochemical potentiokinetic reactivation (EPR) test is based on the assumption that only sensitized grain boundaries become active, while grain bodies are unsensitized. Thus, obtained curve of sensitized stainless steels will be different from the non-sensitized. This constitutes basis of EPR tests.

II.3.1. Acid Tests

Acid tests are used as quality and control or acceptance tests in the industry. However, these bear no direct relations to behavior in service environment, but these tests are able to detect intergranular attack in some specific environments. That is, material may or may not be attacked intergranularly in another environment and also is not predicted resistance to general and pitting corrosion, stress corrosion cracking. The most damaging environments and longer testing periods are selected for limiting acceptance of the material. Acid test methods have been standardized by ASTM and are described in ASTM A262-91 [1], which is summarized in Table II-1.

Table II-1. Summary of ASTM A262 for detecting susceptibility to intergranular attack in austenitic stainless steels [1].

ASTM A262	Test Solution	Test Period	Evaluation	Sensitivity to Phases
Practice A (Oxalic acid)	%10 $H_2C_2O_4$ Ambient temperature	1.5 mins 1 A/cm^2 Anodic	Microscopic	Carbides in 304, 304L, 316, 316L, 316H, 317, 317L, 321, 301, CF-3, CF-3M, CF-8, CF-8M
Practice B (Streicher)	%50 H_2SO_4 + %2.5 $Fe_2(SO_4)_3$ Boiling	1 period of 120 hrs	Weight loss per unit surface area	Carbides in 304, 304L, 316, 316L, 317, 317L, CF-3, CF-8; Carbides and sigma phase in CF-3M, CF-8M, 321
Practice C (Huey)	%65 HNO_3 Boiling	5 periods of 48 hrs each, fresh solution each period	Average weight loss per unit surface area	Carbides in 304, 304L, CF-3, CF-8; Carbides and sigma phase in 316, 316L, 317, 317L, CF-3M, CF-8M, 321, 347
Practice D (Warren)	%10 HNO_3 + %3 HF at 70 °C	2 periods of 2 hrs, fresh solution each period	Weight loss per unit surface area	Carbides in Mo containing steels 316, 316L, 316LN, 316N, 317, 317L
Practice E (Copper accel. Strauss)	%16 H_2SO_4 + %6 $CuSO_4$ Boiling, in contact with metallic copper	1 period of 24 hrs	Macroscopic appearance after bending	Carbides in 201, 202, 301, 304, 304L, 316, 316L, 317, 317L, 321,347
Practice F (Copper accel.)	%50 H_2SO_4 + $CuSO_4$ Boiling, not in contact with metallic copper	1 period of 120 hrs	Weight loss per unit surface area	Carbides in CF-3M, CF-8M

The oxalic acid etch test (ASTM A 262, Practice A) is rapid and nondestructive, but not quantitative. It is a rapid etching procedure and is used for acceptance of material but not rejection of it. That is, rejected specimen should be subjected to the other test's evaluation. In this method, specimens are dipped into 10% oxalic acid solution as an anode and a current density of 1 A/cm^2 is applied at the ambient temperature. If the temperature is increased, stability of passive film is not maintained even for the homogeneous structure of the nonsensitized condition.

The etched structures, which are inspected with scanning electron and/or optical microscope, are classified as [1];

Step: absence of chromium carbides
Dual: no single grain completely surrounded by carbides
Ditch: one or more grain completely surrounded by carbides

The earliest acid test for detecting susceptibility to intergranular corrosion is the copper sulfate-sulfuric acid test (ASTM A 393), known as the Strauss test. In this test method, dissolved Cu^{2+} acts as an activator in sulfuric acid to passivate grains and attacks the chromium depleted grain boundaries. Due to low rate of attack, it is not considered for lower carbon stainless steels. Therefore, it is modified (ASTM A 262 Practice E, Copper-copper sulfate-sulfuric acid test) to increase attack with metallic copper by making stainless steel an anode in a galvanic couple. After 24 hrs testing period, the microstructure is evaluated with the form of bend-test pieces, because disintegration can be readily detected by failure of metal, which has suffered from intergranular attack. Specimens are classified as acceptable or unacceptable according to cracks in bent specimens. Practice F is similar to Practice E, but specimen is not in contact with the metallic copper, which generates cuprous ions for depositing the specimen surface and lowering corrosion potential. Also, weight loss is used for detecting sensitization in Practice F [29].

In other practices (ASTM A262, Practice B - Streicher, Practice C - Huey, Practice D - Warren tests), susceptibility to disintegration is assessed on the basis of weight loss after prescribed period of contact with the test solution. These four tests are quantitative but require testing specimen to be in contact with hot, concentrated acids for periods from 4 hrs to 240 hrs.

Practice C, boiling nitric acid test known as Huey test is the most popular test method. It is also sensitive to susceptibility caused by the sigma phase. The specimens are dipped into boiling 65% nitric acid for five periods of 48 hrs each. In the Huey test, intergranular attack is accelerated due to the presence of hexavalent chromium ions formed due to the oxidation of Cr^{3+} to Cr^{6+} ions. If more than one sample is exposed in the flask, corrosion rate increases considerably [30]. However, it is possible to expose more than one sample, if hexavalent chromium ion concentration does not go beyond 30 ppm [31, 32]. On the other hand, the self acceleration can be considered as an advantage because of increasing the distribution between non-sensitive and sensitive steels [33].

Practice B, ferric sulfate-sulfuric acid test was described by M. A. Streicher and detects only chromium carbides. Corrosion products do not accelerate the corrosion rate. So, it can be run continuously for the whole period of 120 hrs. However, the ferric sulfate should be dissolved in the boiling sulfuric acid solution before specimen is immersed, because, without Fe^{3+} oxidizer, specimens corrode very fast. In addition, ferric sulfate inhibitor may have to be added, if the color of the solution changes to dark green due to excessive corrosion of severely sensitized specimen [33].

Practice D, nitric-hydrofluoric acid test was developed to differentiate between the carbide and sigma phases in molybdenum containing steels by D. Warren. It is enough to have two periods of 2 hrs testing time each, due to increased attack rate with test solution whose temperature must be controlled with attention and kept at 70 °C. In addition, because of high general corrosion rate, it is necessary to compare weight losses of sensitized steel with the non-sensitized [34].

II.3.2. Electrochemical Potentiokinetic Reactivation (EPR) Tests

Electrochemical methods have been used for a variety of purposes in corrosion testing. Also, polarization techniques have been applied for years to characterize the corrosion behavior of metal alloys in specific environments. Extensive cyclic polarization measurements can determine the degree of susceptibility to intergranular corrosion in austenitic stainless steels with polarization curves.

To provide a rapid, quantitative and nondestructive test method, lead many researchers to develop electrochemical potentiokinetic reactivation (EPR) tests. The history and review of EPR method were presented by V. Cihal and R. Stefec [35]. Detection of sensitization of stainless steel started with potentiostatic polarization for etching of grain boundaries by V. Cihal and M. Prazak in 1956. Introduction of reactivation from transpassive or passive state with EPR technique was presented by V. Cihal, A. Desestret, M. Froment, G.H. Wagner in 1969.

Thirty years ago, a need to non-destructively quantify sensitization manifested itself in nuclear reactor piping welds. Clarke *et. al.* found out firstly the single loop EPR test to quantify the sensitization [36]. This technique was also developed by Novak *et. al.* in 1975 [37].

Double loop technique was first attempted by Desestret *et. al.* [38], Knyazheva *et. al.* [39], Charbonier [40], Umemura *et. al.* [41, 42] and Borella and Mignona [43] between the years 1971 - 1980. This technique for especially detecting sensitization of 304 stainless steels was developed by Majidi and Streicher in 1984 [44].

II.3.2.1. Single Loop Test Method

In the single loop test, a sample polished to a 1 micron finish, is polarized for two minutes at 200 mV vs SCE in a solution of 0.5M H_2SO_4 + 0.01M KSCN. Following this step, the potential is decreased at a rate of 6 V/hr to the corrosion potential, $E_{corr.}$ This decrease results in reactivation of

the specimen, involving breakdown of passive film covering chromium depleted regions of material.

The area under the large loop generated in the curve of potential vs current, Figure II-8 is proportional to electric charge, *Q* that depends on surface area and grain size. On non-sensitized material, passive film is intact and size of loop is small.

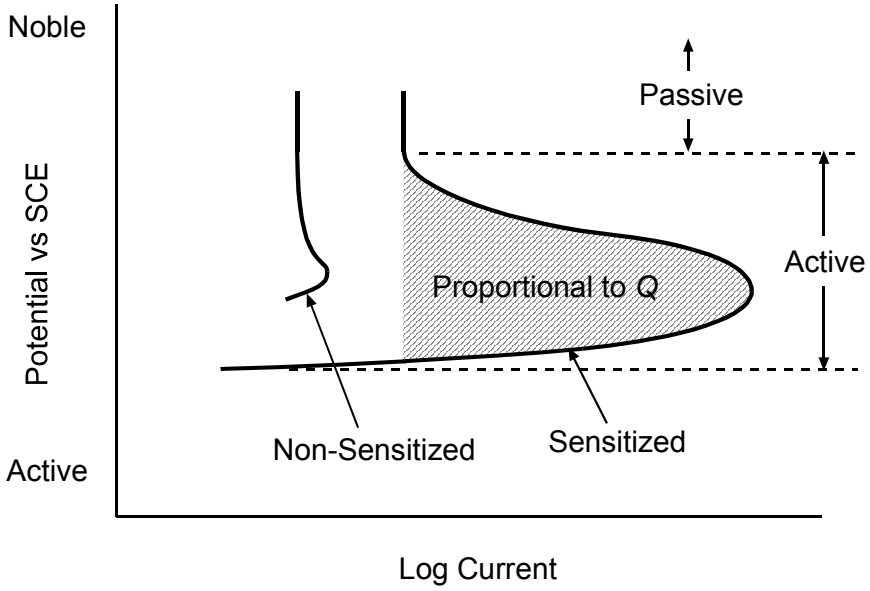

Figure II-8. Sketch for the procedures of single loop EPR test method.

Then *Q* is normalized by total grain boundary area (*GBA*) as seen in equation below,

$$P_a = \frac{Q}{GBA} \quad \left(C/cm^2\right)$$

where, $GBA = A_s\left[5.09544\times10^{-3}\exp\left(0.34696\mathrm{X}\right)\right]$, A_s is the specimen surface area and X is the ASTM grain size number. P_a can be selected as a tolerable level of sensitization for a given application [2].

Although this test has been standardized, there are major difficulties in using single loop EPR test, which are, the necessity of measuring grain size and polishing with 1 micron diamond paste, since reactivation behavior is very sensitive to surface finish. This led to the development of a new procedure that is the double loop test method, which basically sets a reference state of sample's own.

II.3.2.2. Double Loop Test Method

In this test, specimen is first polarized anodically through the active region then the reactivation scan in the reverse direction is carried out. When it is polarized anodically at a given rate from the corrosion potential to a potential in the passive area, this polarization leads to the formation of a passive layer on the whole surface. Then when scanning direction is reversed and the potential is decreased at the same rate to the corrosion potential, it leads to the breakdown of the passive film on chromium depleted areas.

As can be seen in Figure II-9, two loops are generated, an anodic loop and a reactivation loop. Evaluations of this method have shown that I_a is relatively insensitive to sensitization but I_r varies with degree of sensitization. I_r is small for unsensitized specimen whereas for sensitized specimen it increases.

A ratio of maximum current generated in the double loop test (I_r:I_a) is used instead of area under reverse scan in single loop test and it is also not necessary to normalize the ratio of maximum current with the grain size. Moreover, in the double loop method, relatively rough 100-grit finish provides reliable data, which was not enough in the single loop method [41]. In double loop method, since initially the specimen is activated anodically whole

surface of the metal is lost, so surface is cleaned before reactivation scans. If this layer left in place, it covers sensitized grain boundaries thus it can retard reactivation of these boundaries during the reactivation scan.

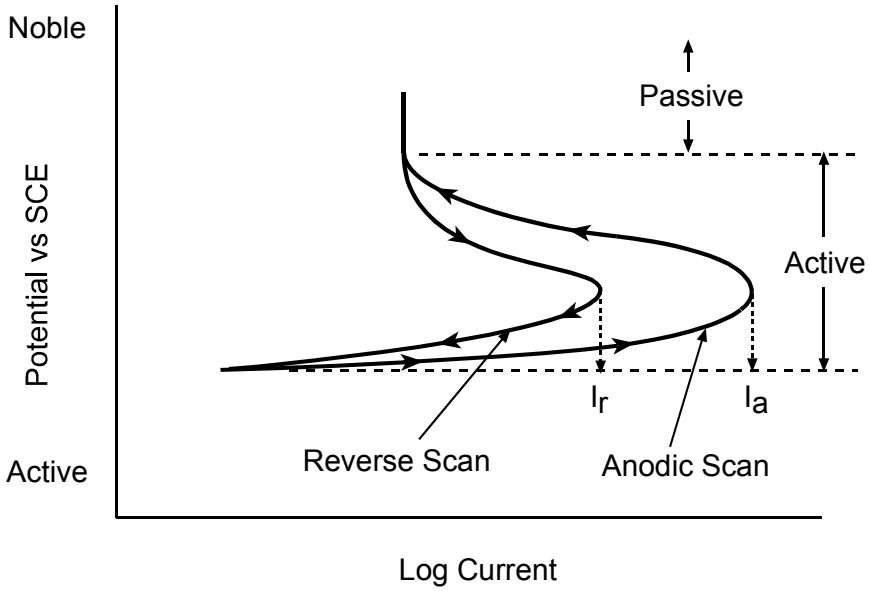

Figure II-9. Sketch for the procedures of double loop EPR test method.

In the literature, there are many studies which deal with verification of EPR test method, comparison of double loop and single loop test methods and improving or applying test methods for different type of materials' susceptibility to intergranular corrosion.

V. Cihal presented a study [45], which was a continuation of an earlier study dealing with electrochemical determination of sensitivity to intercrystalline corrosion of stainless steel, based on reactivation from passive state. He suggested that test method was verified on austenitic

chrome nickel steels with increased carbon content and cold deformed. The ratio of charge during reactivation gave optimum quantitative criterion of tendency of steels to intercrystalline corrosion and intergranular stress corrosion. By changing experimental procedure, this method can be adjusted the other types of steels.

Discrepancies between the standard test (ASTM A262 Practice E) and electrochemical reactivation test method were showed by Novak, Stefec and Franz [37]. They observed that the reactivation method detects both continuous and local chromium depleted region in the steel structure, however acid test exposes only continuous depletion zones leading to intergranular corrosion.

The original work by Majidi and Streicher [44], that proposes the double loop method, compares the results of this new method and the single loop and acid test and concludes that; the agreement between measurement made with DL and SLEPR test was good and gave a quantitative measure of sensitization. It is also concluded that the reproducibility of the DL test is excellent when optimum conditions are maintained. The optimum conditions were determined by examining parameters such as surface finish, scan rate, temperature and KSCN concentration which is used as an activator. They have determined the optimum DLEPR test conditions to be electrolyte of composition 0.5M H_2SO_4 + 0.01M KSCN and a scan rate of 6 V/hr. Some specifics are such that there was an increase not only in intergranular corrosion but also in general corrosion when lower scan rates are used. Another result was increased I_r:I_a ratios as the amount of KSCN concentration increases because there is again general and intergranular corrosion at the entire surface of specimen due to the activator property of KSCN. However, above 0.03M KSCN there is no further increase in I_r:I_a ratios.

Majidi and Streicher also studied the effects of some parameters on P_a values in the single loop method for 304 and 304L type stainless steels. They proposed that P_a value increases when decreasing scan rate, increasing roughness from 1 to 23 micron and temperature of test solution [46].

Similarly for 304 type stainless steels, degree of sensitization was evaluated with single loop method by Jargelius et. al. [47]. They mentioned that EPR test results are strongly dependent on the testing temperature. Increasing temperature increases P_a value.

In the literature, there were also some studies on the applicability of DLEPR method on high nickel alloys like Inconel 600, since this alloy also suffers from intergranular corrosion. Influence of some test parameters on EPR response were investigated in order to assess the optimum conditions which were determined to be 0.1M H_2SO_4 + 0.001M KSCN for sensitivity of EPR test method by Maday and Mignone [48]. They discovered that at too low sulfuric acid concentration chromium depleted regions were not detected, while too high acid concentration caused other types of attack. On the other hand, the optimal modified DLEPR test condition for alloy 600 was obtained in 0.01M H_2SO_4+ 10ppm (0.0001M) KSCN at 25 °C and at 0.5mV/sec scan rate by Ahn *et. al.* [49]. They observed that standard test conditions cause pitting and general corrosion in addition to intergranular corrosion.

On the other hand, the effect of KSCN addition and its concentration on the reactivation behavior at SLEPR test method of Alloy 600 in sulfuric acid solution were investigated by Wu and Tsai [50]. They discovered that at high KSCN concentrations, passivation is enhanced. Tsai, Wu and Cheng also proposed that for sensitized Alloy 600, three anodic peak appear in the reactivation loops. While higher anodic potential correspond to pitting corrosion and matrix corrosion at lower potential. In the potential range of +60 to -10 mV SCE was associated with grain boundary corrosion [51]. However, Roelandt and Vereecken [52] suggested that due to sensitivity of EPR method to pitting attack, differentiation between intergranular corrosion and pitting corrosion from reactivation charge is difficult.

Similarly, the sensitization to intergranular corrosion of AISI 316 type stainless steel was evaluated quantitatively both by microscopically and by electrochemical tests. The conformity of EPR test methods (single and double loop) and Strauss test on 18Cr-12Ni-2.5Mo austenitic stainless steel was examined by Zahumensky and Tuleja [53]. An excellent agreement was

observed between the results of these test methods. They also found that annealing at 650 °C for 100 hours led to the highest sensitization among experimental states [53].

In another study by Matula *et. al.* [54], the degree of sensitization of AISI 316L type stainless steel to intergranular corrosion was determined by means of electrolytic etching in oxalic acid and EPR test method followed by metallographic inspection. Also the kinetics of precipitation of second phases were studied by means of quantitative metallography and first $M_{23}C_6$ carbides at grain boundary were detected. Chromium depletion were quantitatively evaluated by analytical electron microscope. They concluded that chromium depleted zones increases with ageing time

The standard electrochemical electrolyte used in DLEPR method, was modified by adding NaCl to the composition and by increasing the concentration of H_2SO_4 for evaluating sensitization of duplex (austeno-ferritic) and 317L type stainless steel by Lopez and others [55]. Results showed that containing 0.01M KSCN + 2M H_2SO_4 + 0.5M NaCl solution which was used for austenitic stainless steel is too aggressive. Moreover, they proposed that the austenitic stainless steels are more resistant to intergranular corrosion than the duplex stainless steel

Goodwin *et. al.* [56] suggested that the additional peak observed in the polarization curves at –310 mV vs SCE in the double loop reactivation test of 304L and 308L stainless steels, which was realized in 0.01M KSCN + 0.5M H_2SO_4 test solution, is because of the presence of the sigma phase.

Also, for 304 and 308 type stainless steels, some new activators like sodium thiosulfate ($Na_2S_2O_3$), carbamide (H_2NCONH_2), sulfocarbamide (H_2NCSNH_2), thioacetamide (CH_3CSNH_2) were proposed to evaluate susceptibility using electrochemical potentiokinetic reactivation technique. Thioacetamide was proven to be more suitable as an activator than other compounds containing sulfur [57, 58]. Huang, Liu and Chen showed that sulfocarbamide has an appropriate aggressiveness for poor corrosion resistance stainless steel [59] and they also compared with sulfur containing compounds activator by themselves [60]. They all insisted that KSCN

solutions give contradictory results since it causes pitting corrosion as well as intergranular corrosion. However, Cheng *et. al.* [61] showed that, anodic dissolution and self corrosion of ferric (Cr17) and austenitic (Cr18Ni9Ti) stainless steel were accelerated in the solution with organic sulfur containing compounds and the anodic polarization behavior of stainless steels was also changed with various type of organic sulfur containing compounds.

Another approach based on electrochemical measurements was developed by Bühler *et. al.* [62]. They claimed that results of EPR test are influenced by kinetic effects due to potentiodynamic character. So they proposed the electrochemical reactivation test (ERT) method which is carried out by potentiostatic polarization in the passive range and then in the active region. They have determined parameters like polarization time and potential range to prevent dynamic effects on the potentiostatic test.

CHAPTER III

EXPERIMENTAL DETAILS

III.1. Materials and Specimen Preparation

The chemical analyses of the specimens used in this study were determined by Optical Emission Spectroscopy (OES) in KOSGEB and the average values are given in Table III-1. Different heat treatment procedures were applied for AISI 304L and 316L type stainless steels, in order to simulate different degrees of sensitization, details are given in Table III-2 and III-3.

Table III-1. Chemical compositions of AISI 304L and 316L type stainless steels (wt %).

Type	C	Cr	Mo	Ni	Si	Mn	P	S	Fe
304L	0.038	18.33	0.16	8.0	0.379	1.35	0.0394	0.0256	71.05
316L	0.021	16.82	2.44	11.5	0.406	1.50	0.0338	0.0478	66.19

Table III-2. Two heat treatments of 304L type stainless steel.

Name of the specimen	Heat treatment time and temperature
N	Solution annealed at 1050 °C for 40 min + water quench
S	N + at 650 °C 40 min + water quench

Table III-3. Heat treatments of 316L type stainless steel.

Name of the specimen	Heat treatment time and temperature
NS	At 1050 °C 40 min + water quench
S-51	NS + at 650 °C 51 hr + water quench
S-160	NS + at 650 °C 160 hr + water quench
S-233	NS + at 650 °C 233 hr + water quench
S-285	NS + at 650 °C 285 hr + water quench
S-336	NS + at 650 °C 336 hr + water quench
S-406	NS + at 650 °C 406 hr + water quench
S-1000	NS + at 650 °C 1000 hr + water quench

The microstructure of 406 hrs heat-treated sample of 316L type steel was observed by Jeol JEM 100 CX II transmission electron microscope (TEM). TEM specimens were prepared using 20% perchloric acid + 80% methanol at room temperature. The potential was set to 25-26 V and electropolishing was carried out Struers Tenupol 3 Twin Jet.

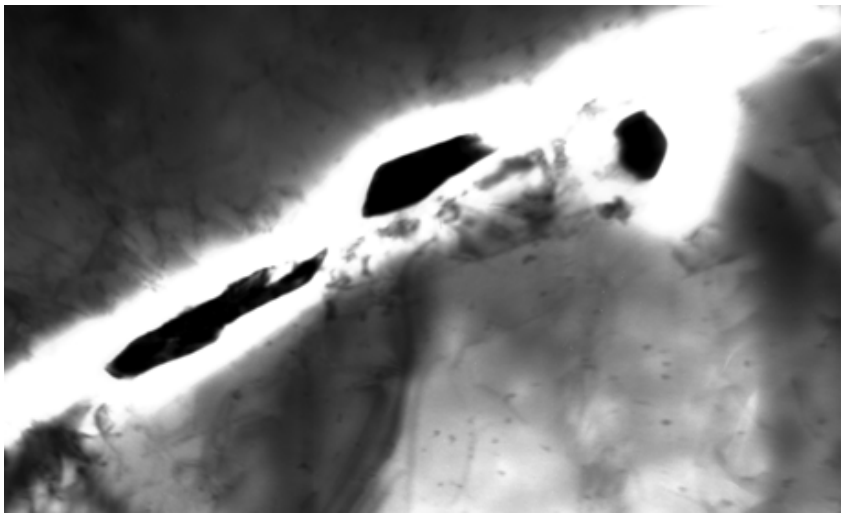

Figure III-1. TEM micrograph of 316L type stainless steel with sensitization heat treatment at 650 °C for 406 hr, X36000 magnification.

It is seen from Figure III-1, that Cr rich second phase particles are aligned along a grain boundary and the boundary region is seen to be bright. This is because of the fact that, during electrochemical polishing the acid attacks chromium depleted regions more, so that these regions become thinner. Therefore electron transparency increases and a bright image outcomes.

The DLEPR specimens are cylindrical in shape and before the heat treatment procedure, first a hole of 2.5 mm diameter was drilled on one side of the 20 mm long samples. Then the regarding heat treatment was applied to specimens after which a 3 mm diameter thread was opened, so that the contact between the specimen and current transfer rod is clear. Finally, all surface of specimen was ground by 400 grit up to 1200 grit emery paper. The finer finish is used for this test to enhance the quality of photomicrographs. And also specimen was polished 3 μm alumina paste for shining appearance. During cutting, grinding and polishing operations work piece was cooled with water to minimize temperature increase. The specimens, S-1000 and S-51, were not evaluated in DLEPR but acid in tests only.

Oxalic acid tests were carried out on 304L and 316L type stainless steels. The microstructural characterization was made by optical and by scanning electron microscopy (SEM) using JEOL JSM-6400 Electron Microscope.

Nitric acid and ferric sulfate-sulfuric acid tests were conducted only for 316L type steel, where all heat-treated samples were used. Especially the nitric acid test result of the long exposure heat-treated samples is important for the determination of sigma phase formation. After heat treatments of 10 mm long specimens, all surface were ground by 120 grit emery paper to remove oxide scale which should be done with care. If a small patch of scale is left, the results can be contradictory.

III.2. Testing Equipment

III.2.1. Weight Loss Acid Tests

1 lt Erlenmeyer flask with 45/40 ground glass joint and four bulbs allihn condenser were used for ferric sulfate-sulfuric acid test, and for nitric acid test 1 lt Erlenmeyer flask with 50 mm neck and cold finger type condenser, were used [1].

III.2.2. DLEPR Test

The electrochemical polarization cell, which is designed according to ASTM G 108 standard [2], see Figure III-2, is a 1 L flask with five necks for working and two auxiliary (counter) electrodes, thermometer, and reference electrode. In this design, the cylindrical working electrode is centrally located between the two counter electrodes which are placed at the sides of the cell for better current distribution and made of materials that are inert to test solution even under strong anodic polarization. In this study, tantalum plates were used as counter electrodes.

The working electrode is mounted in the holder, as shown in Figure III-3 [63]. It can be understood that a threaded stainless steel rod is screwed into a drilled and tapped hole in the specimen electrode. The other end of the rod compresses the specimen towards the tapered teflon gasket, so that the risk of crevice attack in the corrosive electrolyte decreases.

The potential of the working electrode is measured by means of reference electrode. This is achieved with using the luggin probe, which is flexibly mounted to the cell and probe tip was placed near the specimen surface to minimize IR-drop. However, the probe tip cannot be placed too close less than 1mm [29] due to conductivity of electrolyte solution. The electrolyte is carried between the reference and working electrode by the salt bridge. The saturated calomel reference electrode is used as reference electrode, which is positioned in a salt bridge. Saturated calomel reference

electrode is composed of Hg_2Cl_2, mercury and saturated potassium chloride solution and also platinum wire provides electrical connection into corrosion cell. The specimen, two counter electrodes and a calomel reference electrode are connected to Solartron 1480 Multi Channel potentiostat. The potentiostat is controlled by Corrware software, which enables the test variables to be specified and the results to be implemented.

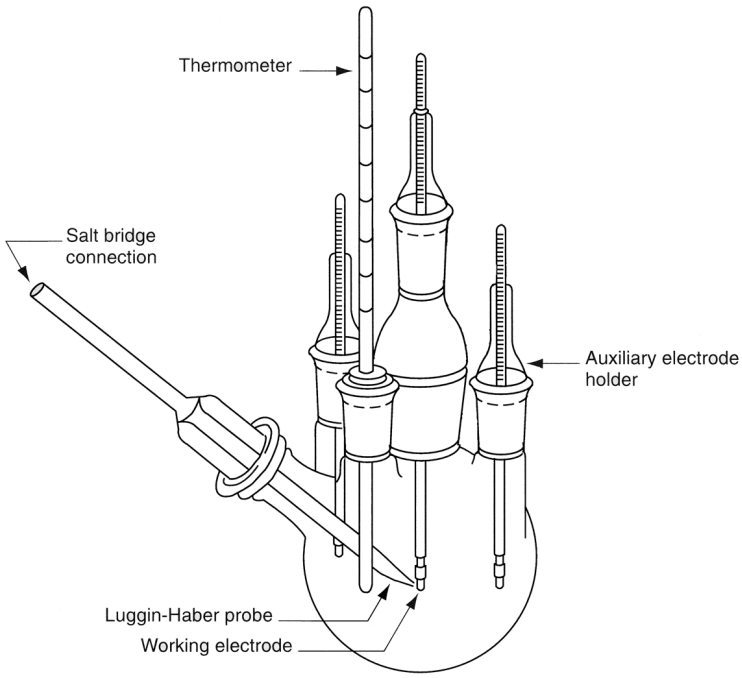

Figure III-2. Electrochemical polarization cell design.

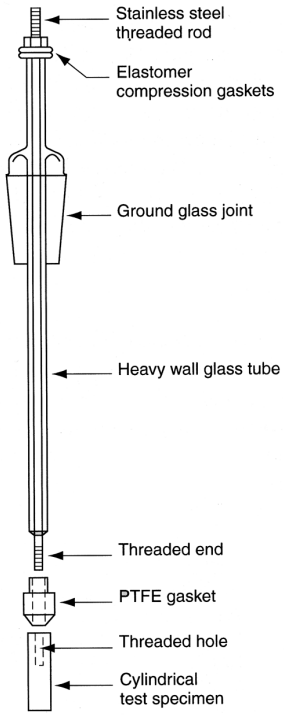

Figure III-3. Specimen electrode mounting.

III.3. Experimental Procedure

III.3.1. Oxalic Acid Test

All specimens were dipped into a solution of 100 gr of oxalic acid crystals ($H_2C_2O_4.2H_2O$) dissolved in 900 ml of deionized water. The specimens were made anode in the stainless steel beaker, which was made the cathode. The specimens were etched at 1 Amp/cm^2 for 1.5 min according to ASTM A 262 Practice A. Before examining with microscopy, etched surfaces were rinsed with deionized water and alcohol and then dried.

III.3.2. Weight Loss Acid Tests

In ferric sulfate-sulfuric acid test ASTM A 262 Practice B, test solution was prepared under the hood. 236 ml of H_2SO_4 is added slowly to 400 ml deionized water in order to prevent boiling by heat evolution so that the concentration of the solution is maintained. Then, 25 gr $Fe_2(SO_4)_3$ is added to sulfuric acid solution. The specimens were not immersed with the cradle in the erlenmeyer flask, before the ferric sulfate was not completely dissolved in the solution. During boiling period of 120 hrs, the color of solution has been controlled and when it changed to dark green, ferric sulfate inhibitor was added.

In nitric acid test ASTM A 262 Practice C, a fresh 65% HNO_3 was boiled and specimens were kept at this condition for a 48 hrs period since among the sensitized specimens, Cr^{+6} development in the solution accelerates the corrosion rate so no further 48 hr periods were carried out.

For acid tests, all 316L type stainless steels with different sensitization degree were weighed with 0.00001 gr sensitivity analytical balance before and after these experiments. The corrosion rate was calculated as the loss in weight per inch per month (ipm) according to ASTM A 262 as follows;

$$ipm = \frac{278 * W}{A * t * d}$$

where, t is the time of exposure in hours, A is the total surface area in cm^2, W is the weight loss in grams and d is the density, where for Cr-Ni-Mo stainless steels it is taken as 8 g/cm^3.

III.3.3. DLEPR Test

For detecting degree of sensitization to intergranular corrosion, potential was controlled precisely by the potentiostat and currents were measured during anodic and reverse scan. Firstly, the specimen was

subjected to open circuit conditions for 5 min so that E_{corr} develops. Then voltage is scanned anodically from E_{corr} to + 0.3 V vs SCE with the regarding scan rate, after which it is reversed back to E_{corr}. The polarization curves were then examined to determine peak currents and charges. After polarization scans bottom sides of the specimen were examined microstructurally by an optical microscope.

The test solution is prepared freshly under a ventilated hood with stirring and used not more than five times due to possible breakdown of solution purity. The solution temperature is held constant at the desired temperature with the use of water bath where its temperature is controlled by thermostated heater. Specimens that are to be used again were ground with 800 and 1200 grit emery paper and polished with 3μm alumina paste.

For 304L type stainless steel, the test parameters were varied according to be Table III-4. After evaluating the results for 304L type stainless steel, it is concluded to keep the solution temperature constant at 30 °C, therefore for 316L type stainless steel the test parameters were varied according to Table III-5.

Table III-4. DLEPR test method parameters for 304L type stainless steel.

H_2SO_4 (M)	KSCN (M)	KCl (M)	T (°C)	Scan (V/hr)
0.5	-	-	25	6
1	-	-	25	6
1.5	-	-	25	6
0.5	-	-	30	6
0.5	0.01	-	25	6
0.5	0.1	-	25	6
0.5	0.01	-	30	6
0.5	0.01	-	40	6
0.1	0.01	-	25	6
1	0.01	-	25	6
1.5	0.01	-	25	6
0.5	0.01	-	25	0.6
0.5	0.01	-	25	60
0.5	-	0.01	25	6
0.5	-	0.1	25	6
0.5	-	0.5	25	6
0.5	-	1	25	6
0.5	0.01	0.5	25	6
0.5	-	-	25	6
0.5	-	-	25	6
0.5	-	-	25	6
0.5	0.01	-	25	6
0.5	-	0.5	25	6
0.5	-	-	25	6
0.5	0.01	-	25	6

Table III-5. DLEPR test method parameters for 316L type stainless steel.

Experiment code	H_2SO_4 (M)	KSCN (M)	Scan Rate (V/hr)
1	0.5	0.005	1
2			3
3			6
4			9
5		0.01	1
6			3
7			6
8			9
9		0.02	3
10			6
11	1.0	0.005	1
12			3
13			6
14			9
15		0.01	1
16			3
17			6
18			9
19		0.02	3
20			6
21	1.5	0.005	6
22		0.01	6
23		0.02	6

CHAPTER IV

RESULTS AND DISCUSSION

IV.1. Test Results for the AISI 304L Type Stainless Steel

The N and S specimens of the AISI 304L steel were determined to have the step and the ditch structures after they have been exposed to oxalic acid test. The microstructures were given in Figure IV-1. As can be seen, N specimen is in non-sensitized condition, whereas the S specimen has been sensitized.

The optimum parameters for the EPR test should represent (to a highest extent) the formation of a passive film all throughout the surface and the breaking down of the film only at the chromium depleted grain boundary regions. The effect of test solution composition, temperature and scan rate on DLEPR, which should therefore be investigated, were given in Table IV-1 for the sensitized and in Table IV-2 for the non-sensitized 304L type stainless steel.

Firstly, the H_2SO_4 concentration was varied (0.5M, 1M and 1.5 M) where the specimens were tested at 25 °C. The polarization curves for the sensitized steel were given in Figure IV-2(a). As can be seen there is an increase in the current of the anodic curve, whereas no appreciable effect is seen on the reactivation curve and in addition I_r is incommensurate. Because of decreasing pH, critical current to reach the passive region during anodic polarization increases, that is, difficult passivation will be realized. In this respect, 0.5M H_2SO_4 can be used instead of high concentration. However, it

is noticed that even with high H_2SO_4 content, passive film could not be broken during the reverse scan. So, it is a necessity to use an activator.

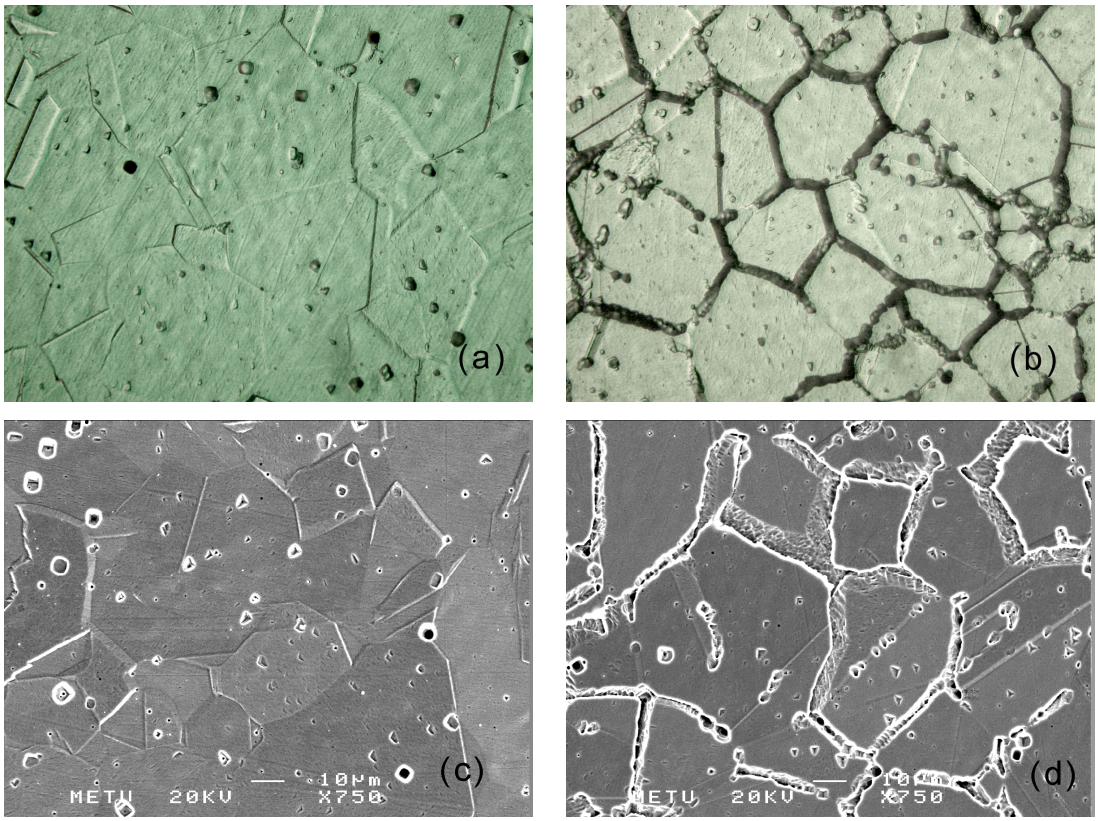

Figure IV-1. Microstructures after oxalic acid test. (a,c) N specimen - step structure, (b,d) S specimen - ditch structure. Optical micrographs are at X500 and SEM micrographs are at X750 magnification.

KSCN was then added as an activator to different molarity H_2SO_4 solutions with varying contents 0.1M, 0.5M, 1M and 1.5 M where the specimens were tested at 25 °C again. The polarization curves for the sensitized steel are given in Figure IV-2(b) for varying KSCN molarity in 0.5M H_2SO_4 solution. It is seen from Table IV-1 that, with 0.01M KSCN addition, the reactivation current becomes commensurable. However, for the S

specimen, there is also an increase in anodic current from $0.174x10^{-3}$ A/cm^2 to $43.587x10^{-3}$ A/cm^2 for 0.5M H_2SO_4. It means that KSCN renders difficult passivation. This property is also clearly noticed, when KSCN increases from 0.01M to 0.1M in 0.5M H_2SO_4 solution. Moreover, going from former to the latter case, a more increase in reactivation charge than reactivation current, may imply an increase in both general corrosion and grain boundary attack. This is actually clearly evident for the non-sensitized case. It is expected that, for the non-sensitized steel, intergranular corrosion should not take place. However during reactivation scans of the N specimen, in solutions containing high KSCN, a more than slight charge develops. It is therefore understood that, KSCN not only activates the grain boundary passive film breakdown, but also increases the general or pitting type of corrosions.

Secondly KCl was used as an activator instead of KSCN in the test solution, because of the capability of aggressive Cl^- ions to break passive films. It is seen that, as KCl molarity is increased, the potential range for passivity gets narrower and the transpassive region comes sooner. So, the stability of passive film was not provided. However in the reverse scan I_r is still incommensurate except in 1M KCl test solution. When both KCl and KSCN were added in the test solution, reactivation current increased considerably even for the non-sensitized steel. This makes it difficult to determine the susceptibility of the steel to intergranular corrosion.

The temperature of the test solution must be carefully controlled if precise comparisons are to be made. The effect can be quite clearly seen in Figure IV-2(c). The I_r:I_a ratio increases about six times when the test solution (0.01M KSCN + 0.5M H_2SO_4) temperature was increased from 25 °C to 40 °C for the sensitized steel. As temperature increases, there is a slight increase in I_r for the non-sensitized steel, but since the increase in I_a is also large, susceptibility of the sensitized steel can easily be differentiated from the non-sensitized.

Scan rate must similarly be chosen carefully since its effect is quite considerable, see Figure IV-2(d). As scan rate is lowered the increase in the reactivation charge is about one order of magnitude larger than the increase

in reactivation current, which means that reverse scan becomes flatter. This may imply more general corrosion which is also seen in non-sensitized steel. In this respect, if scan rate is increased, there may not be enough time to break down the passive film. Thus, misleading results can be obtained.

Table IV-1. DLEPR test results of sensitized 304L type stainless steel.

H_2SO_4 (M)	KSCN (M)	KCl (M)	T (°C)	Scan (V/hr)	Ia (mA/cm^2)	Ir (mA/cm^2)	Qa (mC/cm^2)	Qr (mC/cm^2)	Ir:Ia (x100)	Qr:Qa (x100)
0.5	-	-	25	6	0.174	-	11.639	-	~0	~0
1	-	-	25	6	0.249	-	23.822	-	~0	~0
1.5	-	-	25	6	0.343	-	30.723	-	~0	~0
0.5	-	-	30	6	0.179	-	12.327	-	~0	~0
0.5	0.01	-	25	6	43.587	1.514	2461.738	79.350	3.475	3.223
0.5	0.1	-	25	6	106.035	3.241	8450.774	252.059	3.056	2.983
0.5	0.01	-	30	6	59.568	5.633	3839.949	334.211	9.457	8.704
0.5	0.01	-	40	6	86.386	16.133	7678.625	1047.112	18.676	13.637
0.1	0.01	-	25	6	21.846	0.407	1373.981	20.144	1.861	1.466
1	0.01	-	25	6	63.430	1.269	4372.163	61.653	2.000	1.410
1.5	0.01	-	25	6	65.918	8.120	4722.304	438.122	12.319	9.278
0.5	0.01	-	25	0.6	37.958	7.365	26231.564	4483.784	19.402	17.093
0.5	0.01	-	25	60	47.219	0.073	351.273	0.328	0.154	0.093
0.5	-	0.01	25	6	0.522	-	35.419	-	~0	~0
0.5	-	0.1	25	6	0.391	-	33.067	-	~0	~0
0.5	-	0.5	25	6	1.439	-	95.857	-	~0	~0
0.5	-	1	25	6	2.694	0.096	165.182	4.703	3.579	2.847
0.5	0.01	0.5	25	6	63.785	4.939	4971.435	276.095	7.743	5.554

Table IV-2. DLEPR test results of non-sensitized 304L type stainless steel.

H_2SO_4 (M)	KSCN (M)	KCl (M)	T (°C)	Scan (V/hr)	Ia (mA/cm^2)	Ir (mA/cm^2)	Qa (mC/cm^2)	Qr (mC/cm^2)	Ir:Ia (x100)	Qr:Qa (x100)
0.5	-	-	25	6	0.187	-	11.074	-	~0	~0
1	-	-	25	6	0.246	-	20.034	-	~0	~0
1.5	-	-	25	6	0.320	-	27.704	-	~0	~0
0.5	-	-	30	6	0.235	-	16.177	-	~0	~0
0.5	0.01	-	25	6	44.896	0.004	2432.453	0.340	0.009	0.014
0.5	0.1	-	25	6	102.176	0.032	8781.109	2.039	0.032	0.023
0.5	0.01	-	30	6	60.586	0.034	3191.304	1.692	0.056	0.053
0.5	0.01	-	40	6	87.037	0.103	7391.156	4.750	0.118	0.064
0.1	0.01	-	25	6	20.687	-	1583.203	-	~0	~0
1	0.01	-	25	6	66.937	0.012	4687.361	0.515	0.018	0.011
1.5	0.01	-	25	6	68.806	0.020	3280.714	0.979	0.029	0.030
0.5	0.01	-	25	0.6	42.228	1.164	25200.240	553.760	2.756	2.197
0.5	0.01	-	25	60	41.505	-	310.260	-	~0	~0
0.5	-	0.01	25	6	0.232	-	17.742	-	~0	~0
0.5	-	0.1	25	6	0.406	-	38.753	-	~0	~0
0.5	-	0.5	25	6	1.408	-	80.979	-	~0	~0
0.5	-	1	25	6	2.437	-	151.841	-	~0	~0
0.5	0.01	0.5	25	6	68.704	0.177	4913.007	10.473	0.257	0.213

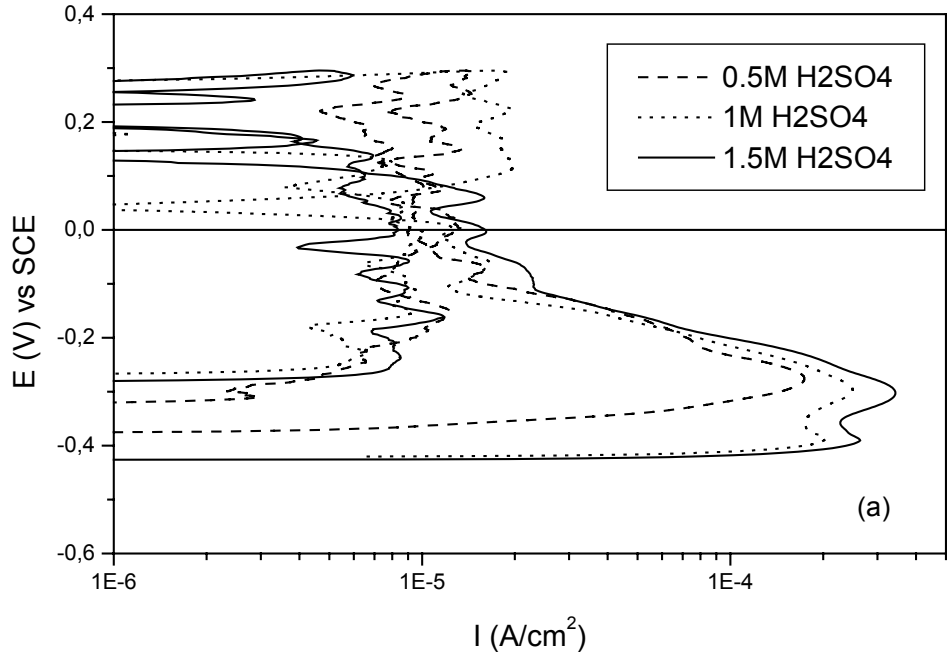

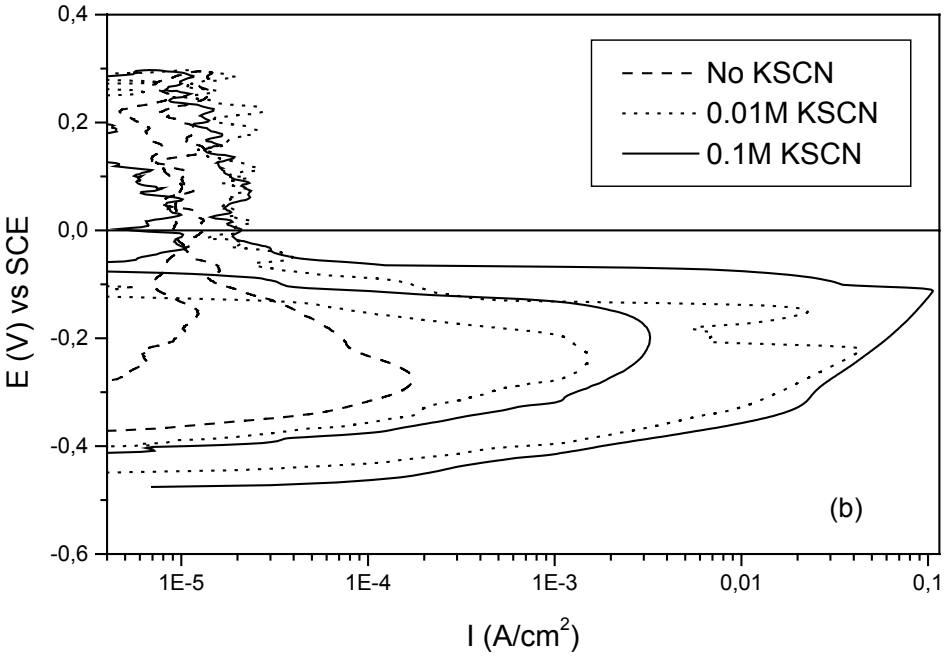

Figure IV-2. The effect of (a) H_2SO_4 molarity, (b) KSCN molarity in 0.5M H_2SO_4, (c) test solution temperature and (d) scan rate on DLEPR test results for sensitized AISI 304L type stainless steel.

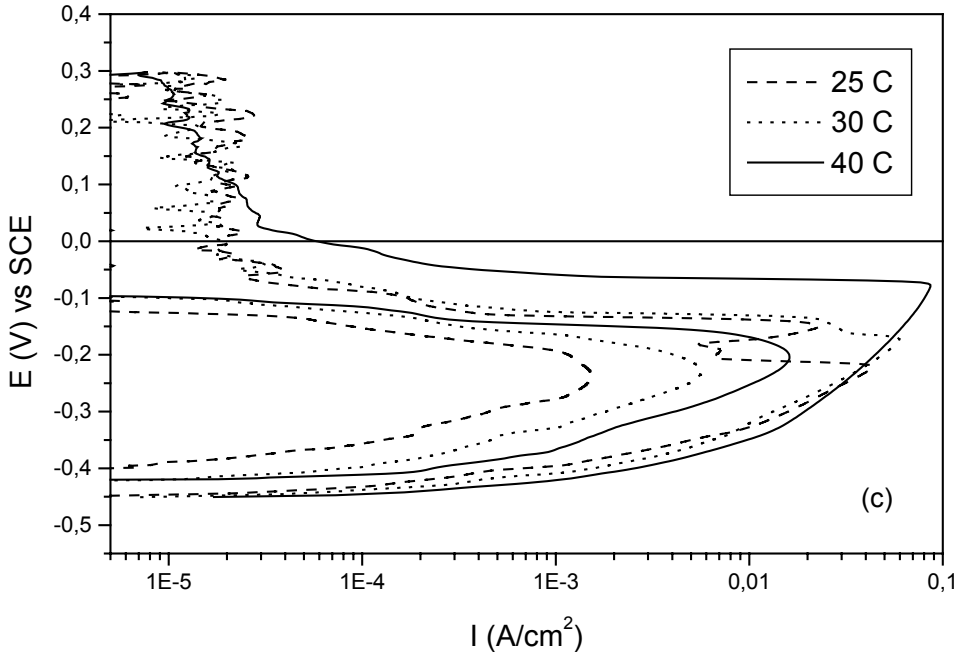

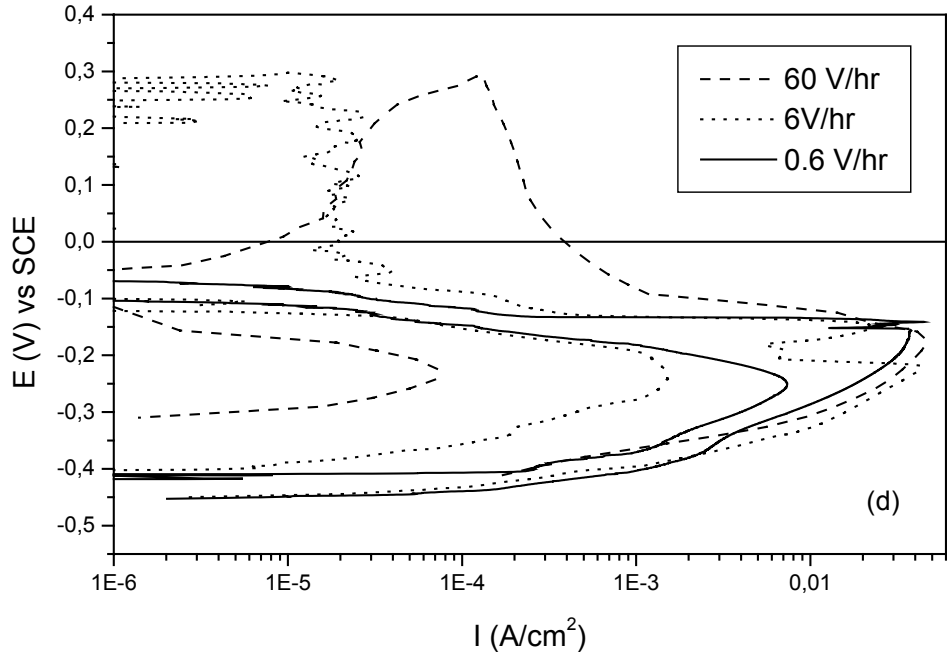

Figure IV-2. Continued.

IV.2. Test results for the AISI 316L Type Stainless Steel

The resulting microstructures after the oxalic acid test were given in Figure IV-3 for the 316L specimens, along with their classification according to ASTM A262. As can be seen, the NS and S-51 specimens exhibit the step structure, whereas S-160, S-233 and S-285 exhibit the dual structure. Although the number of completely encircled grains in S-406 and S-1000 is more than in S-336, both are classified as the ditch structure.

Designing the DLEPR test for the testing of susceptibility to intergranular corrosion in these specimens, solution temperature was kept constant at 30 °C ± 1 °C. The parameters, which are H_2SO_4, KSCN and scan rate, were investigated as was given in Table III-5. In addition to these, KCl effect was also investigated in a solution containing 0.005M KSCN and 0.5M H_2SO_4.

The DLEPR test results for the step structure was given in Table IV-3. In any of the combinations of the test parameters, imperceptible reactivation behavior was obtained, which clearly depicts the state of the structure. However all of the sensitized specimens, of different degree, showed a clearly recognizable reactivation behavior, as it is seen from the polarization curves given Figure IV-4. The results of the DLEPR test for the other specimens were given in Tables IV-4 to IV-8.

In general, what is observed from these tables are that; for all specimens, KSCN is more effective than H_2SO_4 to increase the passivation potential and current almost irrespective of the scan rate used. Moreover, at the same test conditions, all specimens gave very similar activation behavior, which is desired, so that I_a can be used as a reference state for the reactivation behavior. The reactivation current itself, however, showed a quite complex behavior depending on the concentrations of KSCN and H_2SO_4, and the scan rate. Therefore in order to understand the effect these parameters, univariate analysis of variance was performed on the I_r:I_a and Q_r:Q_a values to obtain a General Linear Model (GLM).

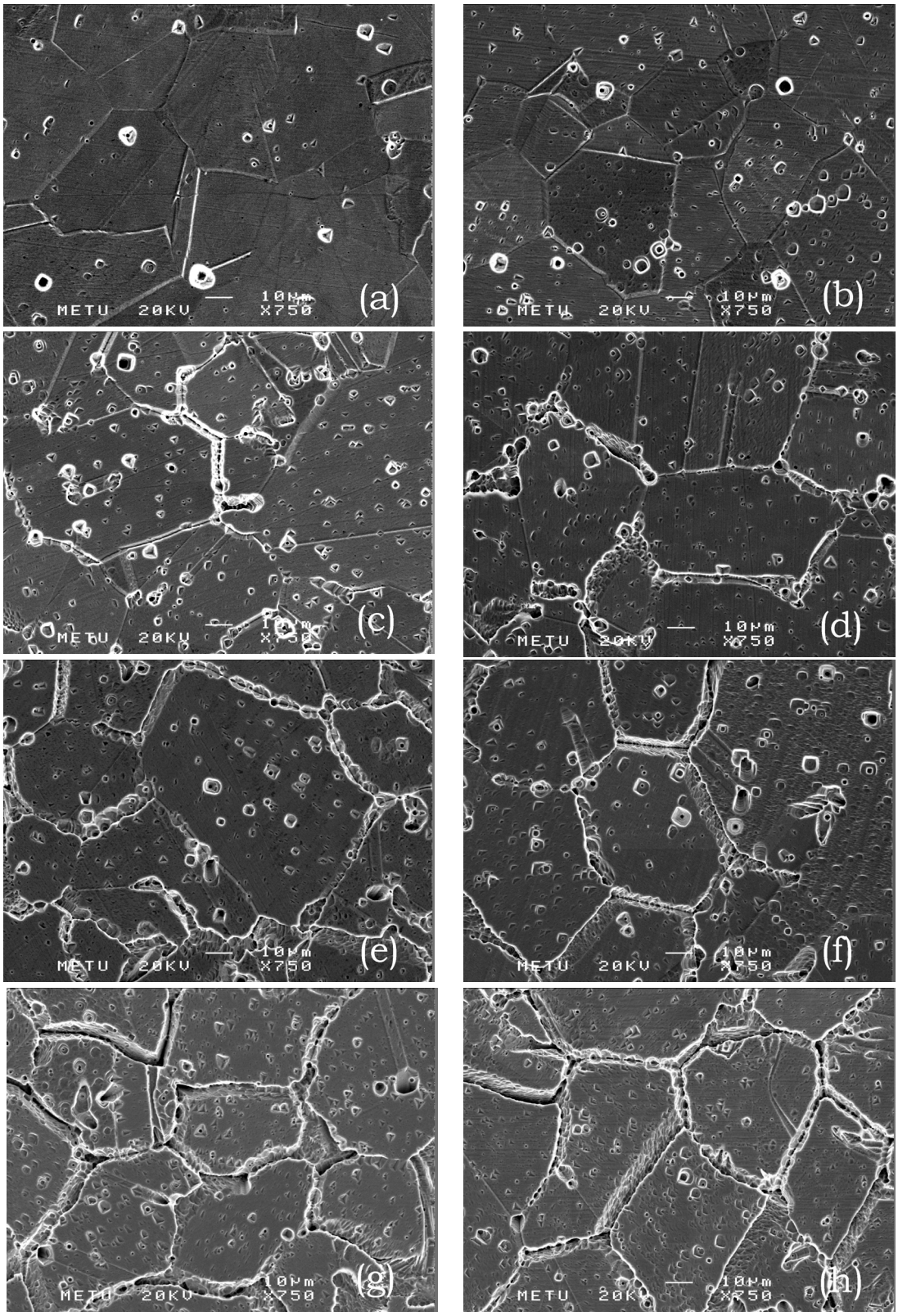

Figure IV-3. SEM micrographs of specimens (at X750 magnification) after the oxalic acid etch. (a) NS – step, (b) S-51 – step, (c) S-160 – dual, (d) S-233 – dual, (e) S-285 – dual, (f) S-336 – ditch, (g) S-406 – ditch and (h) S-1000 – ditch.

Table IV-3. DLEPR test results of NS specimen exhibiting step structure.

H_2SO_4 (M)	KSCN (M)	Scan (V/hr)	Ia (mA/cm^2)	Ir (mA/cm^2)	Qa (mC/cm^2)	Qr (mC/cm^2)	Ir:Ia (x100)	Qr:Qa (x100)
0.5	0.005	9	10.680	0.013	347.232	0.257	0.119	0.074
		6	10.339	0.005	533.808	0.221	0.052	0.041
		3	11.711	0.002	1091.722	1.430	0.189	0.131
		1	12.685	0.007	3640.572	2.372	0.052	0.065
	0.01	9	13.549	0.006	432.647	0.075	0.041	0.017
		6	14.936	0.014	687.108	0.488	0.095	0.071
		3	14.743	0.010	1390.681	0.746	0.068	0.054
		1	16.461	0.014	4738.183	0.880	0.083	0.019
	0.02	6	20.975	0.015	983.370	0.352	0.074	0.036
		3	20.975	0.001	2148.925	0.554	0.003	0.026
1	0.005	9	11.327	0.004	429.620	0.180	0.040	0.042
		6	13.448	0.010	788.509	0.139	0.072	0.018
		3	13.904	0.005	1574.050	0.742	0.036	0.047
		1	12.181	0.025	4428.497	0.796	0.201	0.018
	0.01	9	17.594	0.006	644.153	0.134	0.034	0.021
		6	17.979	0.004	1007.641	0.106	0.021	0.011
		3	17.979	0.011	2188.928	0.384	0.061	0.018
		1	18.682	0.043	6484.081	5.787	0.023	0.089
	0.02	6	26.968	0.004	1524.609	0.022	0.013	0.001
		3	28.467	0.011	3016.556	0.302	0.040	0.010
1.5	0.005	6	12.444	0.018	798.431	0.006	0.148	0.001
	0.01	6	17.979	0.011	1165.106	0.276	0.063	0.024
	0.02	6	28.467	0.008	1757.285	0.394	0.028	0.022

Table IV-4. DLEPR test results of S-160 specimen exhibiting dual structure.

H_2SO_4 (M)	KSCN (M)	Scan (V/hr)	Ia (mA/cm^2)	Ir (mA/cm^2)	Qa (mC/cm^2)	Qr (mC/cm^2)	Ir:Ia (x100)	Qr:Qa (x100)
0.5	0.005	9	11.145	0.312	558.709	12.931	2.797	2.314
		6	10.922	0.609	568.327	41.958	5.579	7.383
		3	12.450	0.264	1206.982	38.494	2.120	3.189
		1	13.156	0.645	3888.082	274.732	4.900	7.066
	0.01	9	15.143	0.163	465.518	6.574	1.080	1.412
		6	14.833	0.228	732.849	14.851	1.538	2.026
		3	16.481	0.572	1608.959	92.034	3.470	5.720
		1	18.279	0.610	5333.283	311.244	3.335	5.836
	0.02	6	20.975	0.102	1107.574	8.900	0.489	0.804
		3	25.470	0.210	2336.055	43.119	0.824	1.846
1	0.005	9	12.151	0.085	472.695	3.388	0.703	0.717
		6	12.663	0.729	752.251	51.895	5.759	6.899
		3	14.026	0.110	1611.656	16.630	0.782	1.032
		1	14.982	0.410	5701.401	209.049	2.735	3.667
	0.01	9	18.491	0.427	688.906	19.222	2.307	2.790
		6	19.441	0.428	1071.556	34.151	2.203	3.187
		3	20.117	0.595	2239.569	95.672	2.956	4.272
		1	23.972	0.668	8410.667	365.466	2.788	4.345
	0.02	6	29.965	0.283	1574.800	22.620	0.945	1.436
		3	32.961	0.629	3631.583	109.548	1.909	3.017
1.5	0.005	6	14.326	0.569	905.491	42.935	3.972	4.742
	0.01	6	19.477	0.644	1238.175	50.191	3.308	4.054
	0.02	6	31.463	0.382	1790.696	31.250	1.214	1.745

Table IV-5. DLEPR test results of S-233 specimen exhibiting dual structure.

H_2SO_4 (M)	KSCN (M)	Scan (V/hr)	Ia (mA/cm^2)	Ir (mA/cm^2)	Qa (mC/cm^2)	Qr (mC/cm^2)	Ir:Ia (x100)	Qr:Qa (x100)
0.5	0.005	9	10.272	0.138	338.258	5.977	1.339	1.767
		6	11.176	0.521	600.255	32.921	4.665	5.484
		3	12.144	0.283	1228.571	43.429	2.332	3.535
		1	14.173	0.710	4354.633	345.614	5.007	7.937
	0.01	9	14.193	0.156	449.262	7.639	1.097	1.700
		6	16.371	0.315	777.721	24.339	1.922	3.130
		3	16.505	0.531	1532.849	86.216	3.219	5.625
		1	19.174	0.659	5241.891	342.438	3.438	6.533
	0.02	6	20.975	0.172	1132.070	15.784	0.821	1.394
		3	23.972	0.375	2391.640	69.442	1.563	2.904
1	0.005	9	12.196	0.269	464.334	13.409	2.202	2.888
		6	13.446	0.797	824.107	48.962	5.930	5.941
		3	14.233	0.302	1635.179	57.189	2.124	3.497
		1	16.630	0.697	6024.421	368.522	4.189	6.117
	0.01	9	17.979	0.247	656.304	12.378	1.375	1.886
		6	17.979	0.610	1076.185	47.936	3.393	4.454
		3	19.477	0.479	2185.033	86.823	2.462	3.974
		1	22.474	1.141	7641.921	598.996	5.077	7.838
	0.02	6	28.467	0.420	1601.169	40.003	1.474	2.498
		3	32.961	0.772	3502.135	146.977	2.341	4.197
1.5	0.005	6	12.706	0.479	782.366	33.225	3.771	4.247
	0.01	6	19.357	0.449	1206.457	40.115	2.319	3.325
	0.02	6	31.463	0.595	1866.207	59.240	1.893	3.174

Table IV-6. DLEPR test results of S-285 specimen exhibiting dual structure.

H_2SO_4 (M)	KSCN (M)	Scan (V/hr)	Ia (mA/cm^2)	Ir (mA/cm^2)	Qa (mC/cm^2)	Qr (mC/cm^2)	Ir:Ia (x100)	Qr:Qa (x100)
0.5	0.005	9	10.638	0.181	353.090	9.000	1.699	2.549
		6	10.924	0.274	494.404	19.628	2.508	3.970
		3	11.536	0.418	1162.604	67.016	3.623	5.764
		1	14.083	0.764	4471.796	427.283	5.426	9.555
	0.01	9	16.007	0.428	599.685	22.984	2.674	3.833
		6	16.010	0.255	812.106	21.369	1.591	2.631
		3	16.031	0.521	1605.514	88.083	3.251	5.486
		1	19.864	1.089	6302.644	620.196	5.485	9.840
	0.02	6	20.975	0.479	1075.931	48.783	2.286	4.534
		3	23.972	0.599	2296.502	138.632	2.500	6.037
1	0.005	9	12.945	0.603	506.405	32.124	4.662	6.343
		6	12.798	0.503	756.117	35.675	3.932	4.718
		3	13.973	0.506	1596.674	91.342	3.623	5.721
		1	15.135	1.155	5393.662	646.520	7.632	11.987
	0.01	9	17.979	0.475	673.863	25.584	2.640	3.797
		6	19.222	0.643	1088.441	55.260	3.344	5.077
		3	19.993	0.695	2239.269	126.027	3.477	5.628
		1	25.470	1.151	8794.966	694.374	4.519	7.895
	0.02	6	28.467	0.669	1646.415	65.496	2.350	3.978
		3	32.368	1.401	4321.073	253.053	4.328	5.856
1.5	0.005	6	12.865	0.573	750.543	42.498	4.455	5.662
	0.01	6	20.442	0.888	1232.946	78.207	4.346	6.343
	0.02	6	30.414	0.584	1781.706	56.746	1.921	3.185

Table IV-7. DLEPR test results of S-336 specimen exhibiting ditch structure.

H_2SO_4 (M)	KSCN (M)	Scan (V/hr)	Ia (mA/cm^2)	Ir (mA/cm^2)	Qa (mC/cm^2)	Qr (mC/cm^2)	Ir:Ia (x100)	Qr:Qa (x100)
0.5	0.005	9	10.787	0.493	363.877	23.211	4.569	6.379
		6	10.652	0.714	463.990	52.957	6.704	11.413
		3	11.686	0.661	1199.296	118.723	5.652	9.899
		1	14.383	1.094	4605.439	661.338	7.604	14.360
	0.01	9	15.200	0.334	494.988	16.716	2.200	3.377
		6	16.015	0.434	778.995	38.385	2.713	4.927
		3	16.442	1.075	1586.336	208.705	6.538	13.156
		1	17.979	1.064	5920.443	698.075	5.917	11.791
	0.02	6	22.474	0.494	1049.037	50.416	2.200	4.806
		3	23.972	0.487	2246.910	109.821	2.031	4.888
1	0.005	9	12.780	0.749	492.936	40.452	5.862	8.206
		6	13.954	0.903	820.391	72.527	6.468	8.841
		3	14.533	0.836	1700.052	160.357	5.753	9.432
		1	15.615	0.884	5588.583	581.392	5.661	10.403
	0.01	9	18.578	0.521	690.044	28.131	2.806	4.077
		6	19.477	0.869	1086.688	76.954	4.462	7.082
		3	20.975	1.314	2340.100	249.861	6.264	10.677
		1	24.089	1.683	8156.117	976.298	6.985	11.970
	0.02	6	28.467	0.719	1621.095	76.860	2.526	4.741
		3	34.205	1.783	3661.698	370.664	5.212	10.123
1.5	0.005	6	13.533	1.117	861.922	84.149	8.251	9.763
	0.01	6	19.477	1.177	1279.227	100.518	6.043	7.858
	0.02	6	31.014	0.824	1787.999	85.849	2.657	4.801

Table IV-8. DLEPR test results of S-406 specimen exhibiting ditch structure.

H_2SO_4 (M)	KSCN (M)	Scan (V/hr)	Ia (mA/cm^2)	Ir (mA/cm^2)	Qa (mC/cm^2)	Qr (mC/cm^2)	Ir:Ia (x100)	Qr:Qa (x100)
0.5	0.005	9	10.952	0.294	360.446	14.083	2.681	3.907
		6	11.062	1.024	562.829	72.766	9.257	12.929
		3	13.230	1.238	1340.385	214.039	9.354	15.968
		1	15.904	1.325	4882.313	774.095	8.333	15.855
	0.01	9	14.655	0.288	485.714	14.237	1.967	2.931
		6	14.982	1.049	809.769	98.319	7.000	12.142
		3	18.175	1.247	1729.867	231.268	6.863	13.369
		1	19.477	2.023	6274.028	1200.554	10.385	19.135
	0.02	6	22.474	0.531	1032.467	49.592	2.361	4.803
		3	23.972	0.674	2169.451	155.697	2.813	7.177
1	0.005	9	13.539	0.959	519.290	43.092	7.083	8.298
		6	13.715	1.706	782.905	131.972	12.442	16.857
		3	15.342	0.805	1804.030	162.619	5.244	9.014
		1	16.229	1.408	5798.637	839.658	8.678	14.480
	0.01	9	19.124	0.361	699.708	18.927	1.885	2.705
		6	19.477	1.168	1159.308	100.207	5.996	8.644
		3	22.354	1.512	2471.945	319.724	6.765	12.934
		1	21.844	1.275	8173.796	790.771	5.835	9.674
	0.02	6	31.444	1.214	1626.938	115.856	3.860	7.121
		3	34.460	1.618	3906.210	372.942	4.696	9.547
1.5	0.005	6	13.774	1.437	882.029	116.843	10.431	13.247
	0.01	6	20.658	0.734	1271.032	74.253	3.554	5.842
	0.02	6	32.362	0.596	1892.426	55.920	1.843	2.955

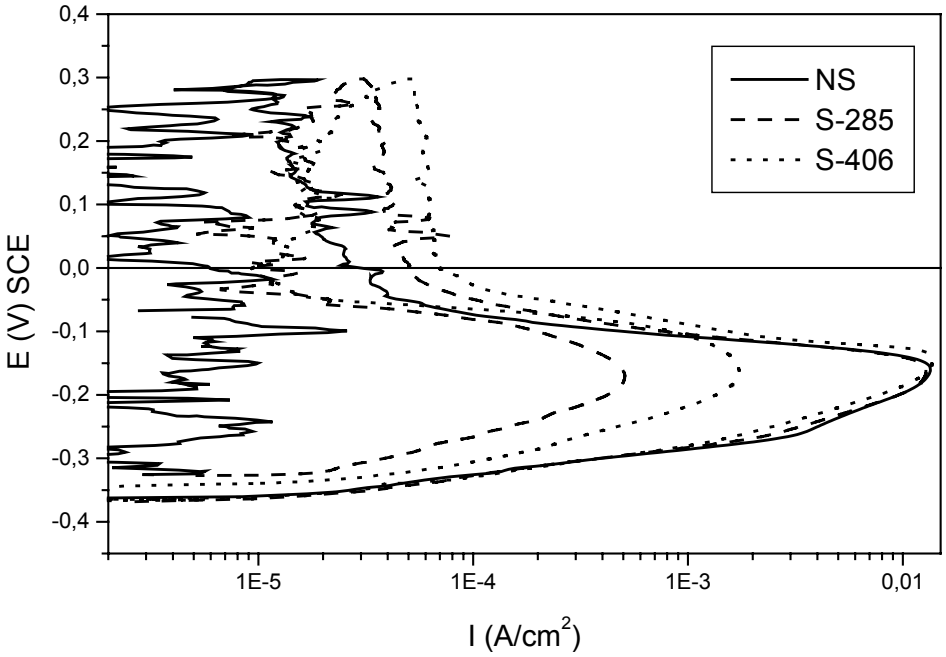

Figure IV-4. Polarization curves for the NS, S-285 and S-406 specimens. Test conditions were 0.005M KSCN + 1M H_2SO_4 and 6 V/hr scan rate.

The GLM Univariate procedure, as implemented in many commercial statistical analysis software like SPSS, provides regression analysis and analysis of variance for one dependent variable by one or more factors and/or variables. Using this General Linear Model procedure, one can test null hypothesis about the effects of other variables on the means of various groupings of a single dependent variable. Therefore one can investigate interactions between factors as well as the effects of individual factors, some of which may be random. In Figure IV-5, for example, Q_r:Q_a ratios (the dependent variable) were plotted for the S-285 and S-406 specimens under all conditions of the test parameters (factor variables). From this figure understanding the effect of one parameter, say e.g. KSCN concentration, may be difficult. However univariate analysis provides error estimates for each factor, and its effect on the dependent variable, see Figure IV-6.

Furthermore the test of null hypothesis gives the importance of the factors' effect. If the significance of the test is lower that 0.05 then it should be understood that the effect of the factor is very significant. In Table IV-9, the significance of the GLM analysis were given for the dependent variables I_r:I_a and Q_r:Q_a for all of the specimens.

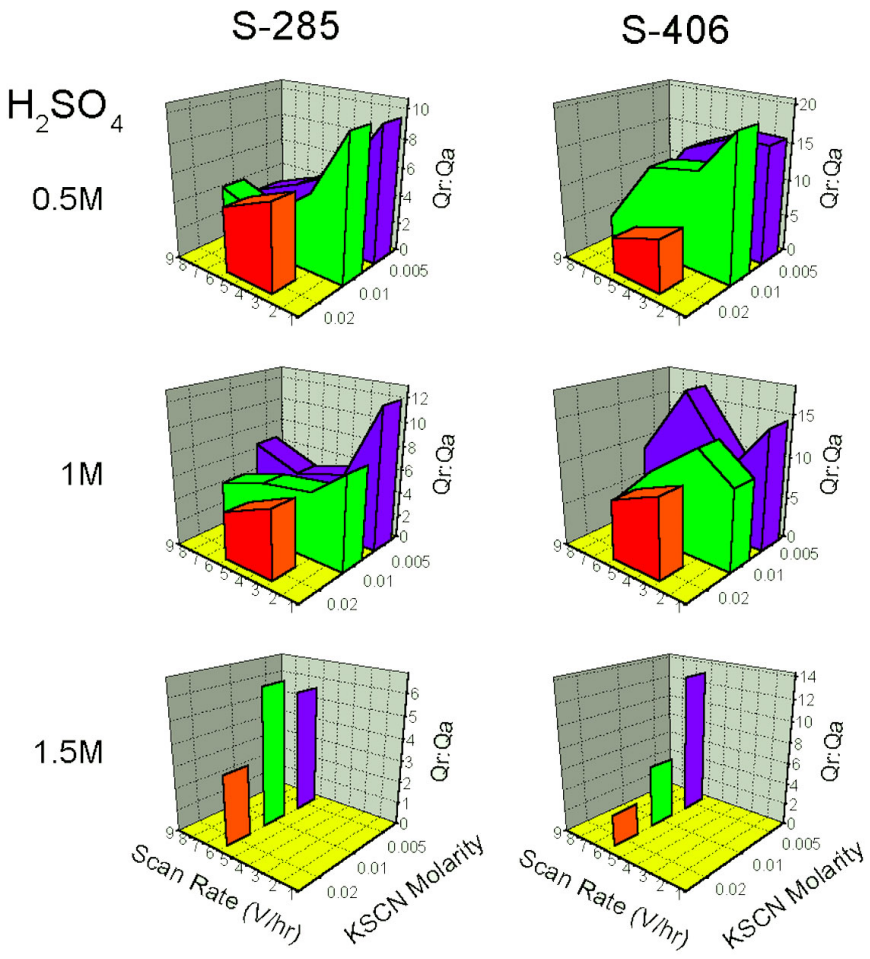

Figure IV-5. Dependence of Q_r:Q_a values on the test parameters for S-285 and S-406.

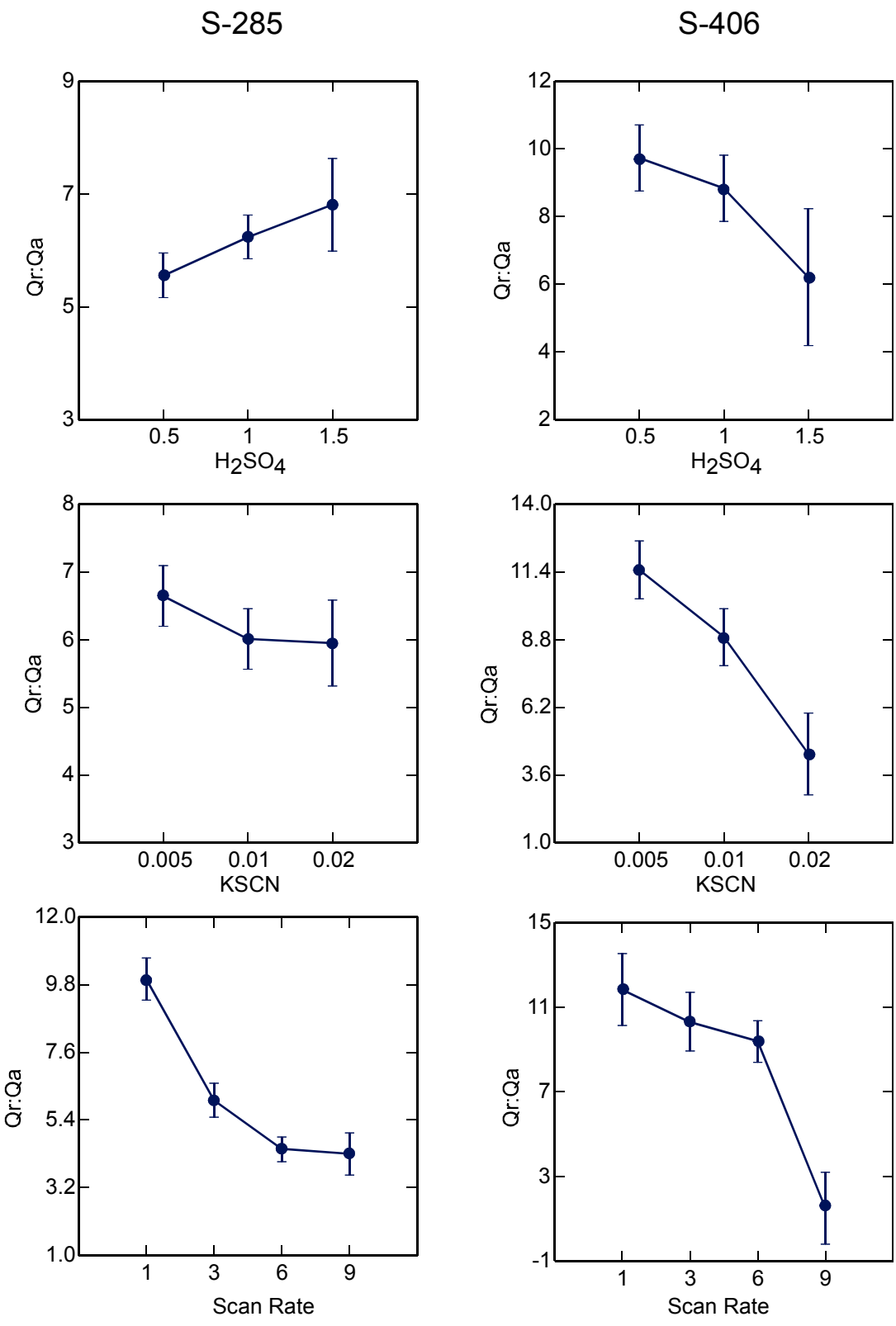

Figure IV-6. GLM analysis factors affecting Q_r:Q_a for S-285 and S-406.

Table IV-9. GLM significance values.

		H_2SO_4	KSCN	Scan Rate
S-160	I_r:I_a	0.873	0.024	0.220
	Q_r:Q_a	0.729	0.058	0.073
S-233	I_r:I_a	0.413	0.009	0.003
	Q_r:Q_a	0.740	0.049	0.000
S-285	I_r:I_a	0.035	0.096	0.001
	Q_r:Q_a	0.270	0.454	0.000
S-336	I_r:I_a	0.149	0.000	0.019
	Q_r:Q_a	0.935	0.010	0.001
S-406	I_r:I_a	0.568	0.001	0.010
	Q_r:Q_a	0.293	0.004	0.001

The analysis of Table IV-9, Figure IV-6 and such figures of all of the specimens for the dependent variable I_r:I_a and Q_r:Q_a, resulted in the following conclusions to be made. The H_2SO_4 concentration has a weak effect on I_r:I_a and Q_r:Q_a regardless of the state of the specimen (dual or ditch) and randomly either increases or decreases them. The KSCN concentration, however, has strong effects on both of the dependent variables, such that increased KSCN always decreases them. The strength of the effect somehow decreases going from ditch to dual structure. Finally, scan rate also has a very strong effect, such that increasing scan rate always decreases I_r:I_a and Q_r:Q_a and the strength of the effect remains regardless of the state of the structure.

If the GLM analysis were made to see the effects of factor variables on I_a and I_r separately, following conclusions can be made. Other factors being constant and regardless of the state of the specimen, the increased concentration of H_2SO_4 causes an increase on both I_a and I_r, as can be understood from its weak effect on the ratio of I_r:I_a. Moreover, going from dual to ditch structure it was observed that, the absolute values of I_a did not change considerably for the respective concentrations of H_2SO_4, whereas, there was a slight increase in the absolute values of I_r.

The effect of scan rate on I_a, other factors being constant, was quite low for all states of the specimen, but there a slight decrease can be noticed when scan rate is increased. Its effect on I_r, on the other hand, is very pronounced and as scan rate increases, I_r drops considerably. Similarly, the absolute values of I_a did not show much dependence on the state of the specimen, but for I_r, there was again a slight increase as going from dual to ditch structure. In addition, it was observed that, the reactivation curve expanded to active potentials with lower scan rates. This can be the sign of an increase in general corrosion rather than intergranular corrosion. The low I_r values at high scan rates, is most probably because of the insufficient time, where the passive film breakdown can not occur effectively during reactivation scan. Therefore, I_a being almost an invariant and strong dependence of I_r on scan rate, it is very probable to come to wrong conclusions about the state of the steel.

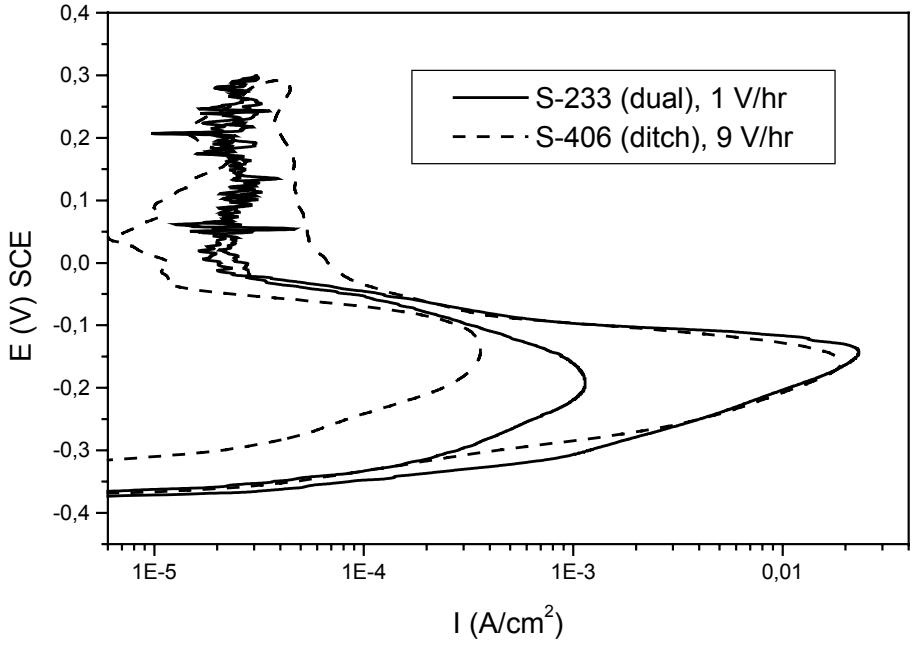

Figure IV-7. Effect of scan rate on the polarization behavior of S-233 and S-406 specimens. Test solution concentration was 0.5M H_2SO_4 and 0.01M KSCN.

In Figure IV-7, the polarization curves of S-233 and S-406 were given, in which the dual structure was appeared to be exposed to more corrosion attack although its grain boundaries are more resistant to intergranular corrosion than the ditch structure.

The effect of KSCN concentration especially on I_r was found to be somehow different from the other factors. Its effect on I_a, others being constant, was such that I_a increases considerably as KSCN molarity increases. This increase was observed for all specimens and the absolute values at respective KSCN concentrations were similar. Its effect on I_r, however, was different. It was observed that at high concentrations of KSCN I_r drops. More important than the drop itself was the change in the reactivation profile. In Figure IV-8, reactivation profiles for the dual and ditch structures were given depending on the KSCN concentration. It can be seen that as KSCN increases there is a drop in the Ir, but also the profile became skewed to higher potentials.

This is very prominent especially in the ditch structure. The reason for this effect may be explained by the observation of a similar effect that was made in Inconel 600 alloy [50, 51]. In that study, the reactivation curve having two distinguishable peaks were deconvoluted to several reactivation curves. Wu *et. al.* [50, 51] arrived to the conclusion, by comparing the microstructure of the alloy that showed the two peak and the one that not, that the peaks were due to different type of corrosions occurring in the alloy. The deconvoluted curve appearing at higher potentials were attributed to the pitting type of corrosion occurred in the alloy.

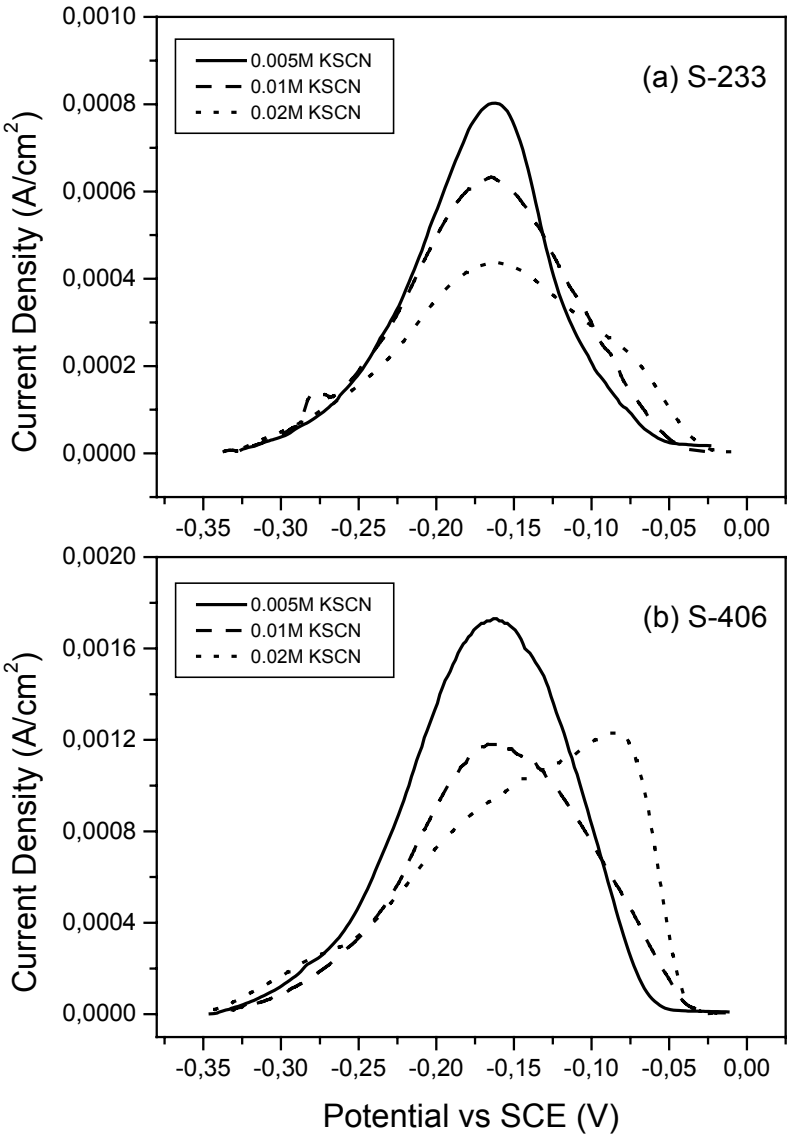

Figure IV-8. Reactivation profiles of specimens (a) S-233 and (b) S-406 during the DLEPR test with different KSCN concentrations.

In this regard, the skewed reactivation profile we obtained, can be because of the combined behavior of two corrosion processes taking place simultaneously, where the one taking place at higher potentials dominating over the other one. Considering the conclusion of Wu *et. al.* [50, 51], we have investigated the microstructure of the S-406 specimen, after it has been

exposed to DLEPR test with different KSCN concentrations. The micrographs were given in Figure IV-9. It can be seen from Figure IV-9 that, there is definitely a different activity taking place at the surface of the specimen, which is not rather the intergranular corrosion. However this activity could not clearly be attributed to pitting type of corrosion, but may be to metastable pits either because of the microstructural features of the alloy or the repassivation mechanism, where the latter seems more likely. As can be seen the number of stable pits observed in low and high KSCN solutions is not so different.

When KCl was added to test solution of 0.005M KSCN and 0.5M H_2SO_4 at 6 V/hr scan rate, it was seen that both activation and reactivation currents have been increased. Activation current values increased about three times, whereas reactivation current values increased less, see Table IV-10. Therefore, a drop in I_r:I_a was realized.

Table IV-10. DLEPR test results of specimens in 0.5M H_2SO_4 + 0.005M KSCN solution containing 0.5M KCl at 6 V/hr.

Specimen	Ia (mA/cm^2)	Ir (mA/cm^2)	Qa (mC/cm^2)	Qr (mC/cm^2)	Ir:Ia (x100)	Qr:Qa (x100)
NS	25.470	0.021	1230.040	0.734	0.082	0.060
S-160	28.467	0.771	1276.500	24.710	2.708	1.936
S-233	29.240	0.735	1274.702	30.315	2.513	2.378
S-285	30.339	0.496	1360.132	9.532	1.635	0.701
S-336	28.248	1.487	1364.222	55.472	5.265	4.066
S-406	29.894	2.670	1329.748	188.389	8.930	14.167

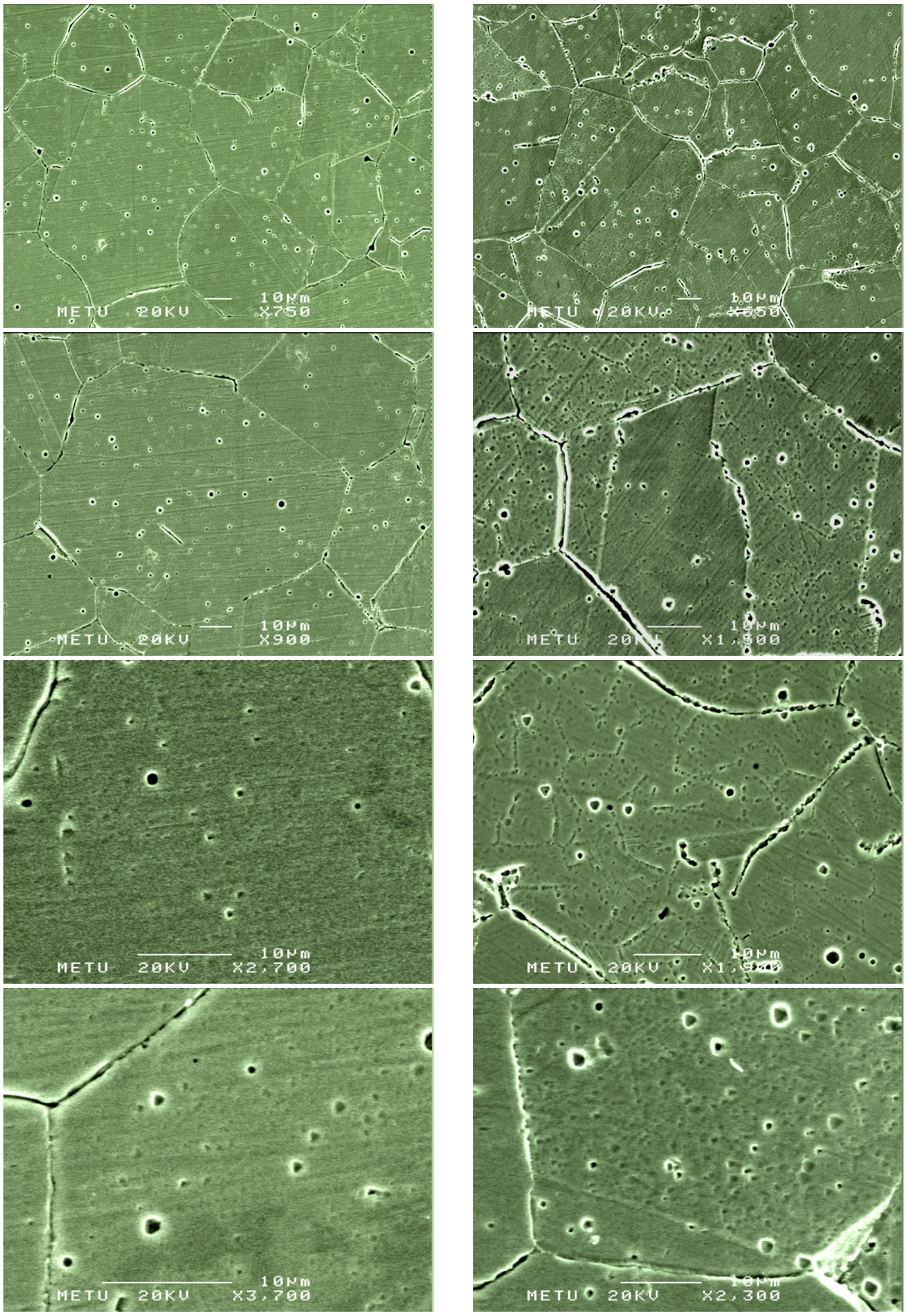

0.005 M KSCN 0.02M KSCN

Figure IV-9. SEM micrographs of S-406 specimen after DLEPR test, (left hand side) 0.005M and (right hand side) 0.02M KSCN.

IV.2.1. Weight Loss Acid Test Results

Results of nitric acid and ferric sulfate – sulfuric acid test methods were given in Table IV-11 and in Figure IV-10.

Table IV-11. Weight loss acid test results of 316L according to ASTM A 262.

Specimen	Practice B	Practice C
	ipm	***ipm***
NS	0.00150	0.00166
S-51	0.00416	0.02952
S-160	0.01244	0.15747
S-233	0.02690	0.19809
S-285	0.05570	0.24414
S-336	0.06413	0.27584
S-406	0.06481	0.24816
S-1000	0.06208	0.25801

Both acid tests gave similar results. Corrosion rate initially increases with ageing time, however, beyond 336 hrs corrosion rate slowed down and even a slight decrease was seen. This is believed to be due to chromium re-enrichment of the grain boundaries because of the availability of time for chromium to diffuse from the grain to the boundary. Moreover, the decrease of the corrosion rate at prolonged times, especially in nitric acid test, may also be an indication of non-existence of the sigma phase, since nitric acid test is sensitive to the presence of sigma.

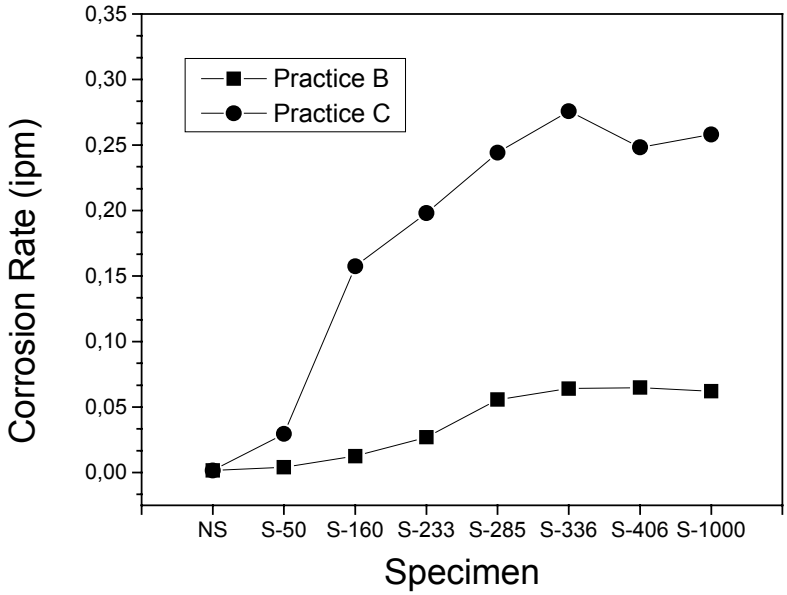

Figure IV-10. Weight loss acid test results of 316L according to ASTM A 262

The main aim of this study was to determine the susceptibility to intergranular corrosion in AISI 316 stainless steel using DLEPR method. Therefore the results of DLEPR method must somehow predict, in the right manner, the state of the specimen as does the weight loss acid tests. In this regard, in order to determine what combination of DLEPR test parameters would give the best prediction, we correlate the results of the DLEPR and weight loss acid tests. The results were given in Table IV-12. The correlation coefficients close to one indicates that the two results are correlated to each other and the significance (less than 0.05) gives how strong is the correlation.

Table IV-12. Correlation between DLEPR and weight loss acid tests.

Correlation (significance)	Practice B	Practice C
Experiment code	Ir:Ia	Ir:Ia
1	0,867 (0,025)	0,946 (0,004)
2	0,862 (0,027)	0,738 (0,094)
3	0,637 (0,174)	0,722 (0,105)
4	0,649 (0,163)	0,749 (0,087)
5	0,874 (0,023)	0,802 (0,055)
6	0,851 (0,032)	0,87 (0,024)
7	0,698 (0,123)	0,597 (0,211)
8	0,91 (0,012)	0,912 (0,011)
9	0,944 (0,005)	0,908 (0,012)
10	0,989 (0)	0,869 (0,025)
11	0,928 (0,008)	0,876 (0,022)
12	0,98 (0,001)	0,871 (0,024)
13	0,667 (0,148)	0,706 (0,117)
14	0,983 (0)	0,837 (0,037)
15	0,881 (0,02)	0,954 (0,003)
16	0,898 (0,015)	0,865 (0,026)
17	0,892 (0,017)	0,897 (0,015)
18	0,703 (0,119)	0,875 (0,023)
19	0,98 (0,001)	0,951 (0,004)
20	0,938 (0,006)	0,851 (0,032)
21	0,871 (0,024)	0,825 (0,043)
22	0,814 (0,049)	0,903 (0,014)
23	0,841 (0,036)	0,968 (0,002)

We set the lower limit of correlation coefficient (for the I_r:I_a) to be 0.9 that is to be satisfied for all acid test, or 0.95 for one test and 0,85 for the other acid test. The DLEPR test parameters that yielded good correlation between the acid tests according to the above criteria were given with the experiment codes 8, 9, 10, 12, 15 and 19. The I_r:I_a ratios of the above mentioned experiments and the *ipm* of Practice B and Practice C for all specimen types were given in Figure IV-11. Experiments 8 and 15 have been

carried out with scan rates 9 and 1 V/hr, respectively. As we discussed before, very high or very low scan rates may be deceptive for the determination of the state of the specimen and it is wise not use these scan rates along with any other test parameter even if it yields good correlation. Moreover the I_r:I_a ratios of the experiment 8, regarding the specimen state, are close to each other, so that the resolution of this particular experiment is low.

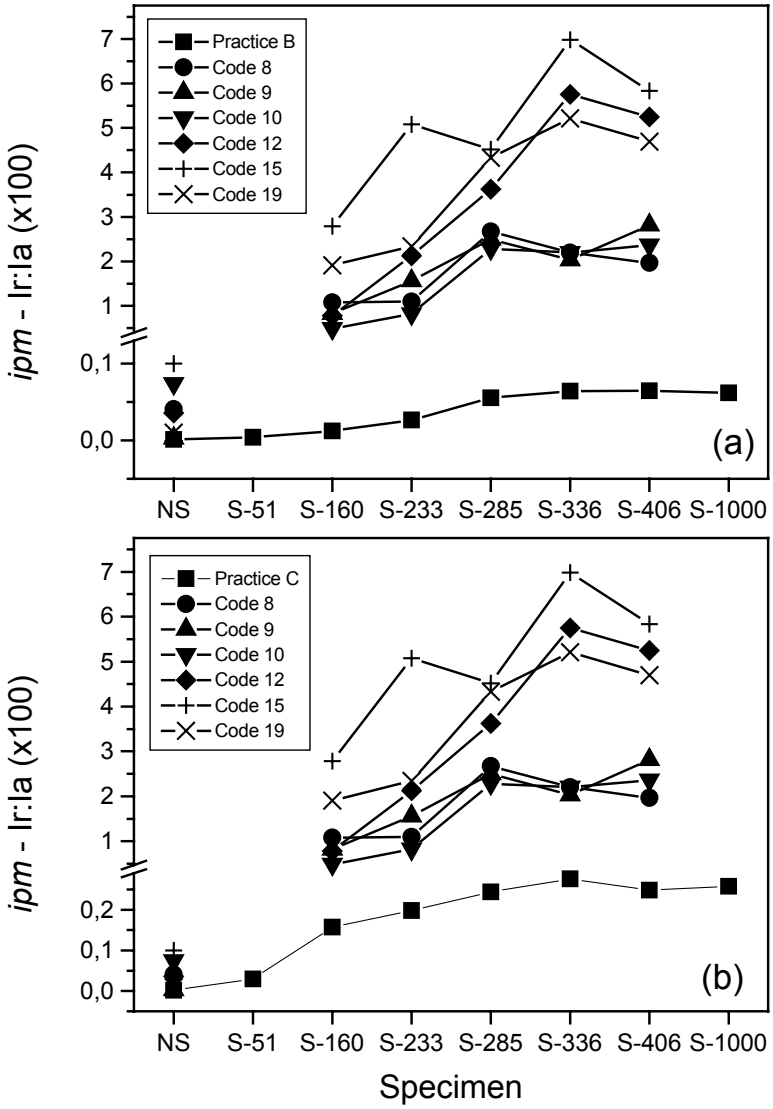

Figure IV-11. Ir:Ia ratios and corrosion rates according to (a) Practice B and (b) according to Practice C.

In the experiments 9, 10 and 19, solutions containing 0.02M KSCN were used. In this condition, we should keep in mind that, during reactivation scan, not only intergranular corrosion but also pitting type of corrosion may take place. This is seen more obviously in the ditch structure rather than in the dual structure, so sensitization degree of the ditch structure should appear to be higher, where this behavior is not inconvenient for our purposes. However, as can be seen from Figure IV-11, for experiments 9 and 10, due to their low H_2SO_4 content, their resolution again seemed to be low.

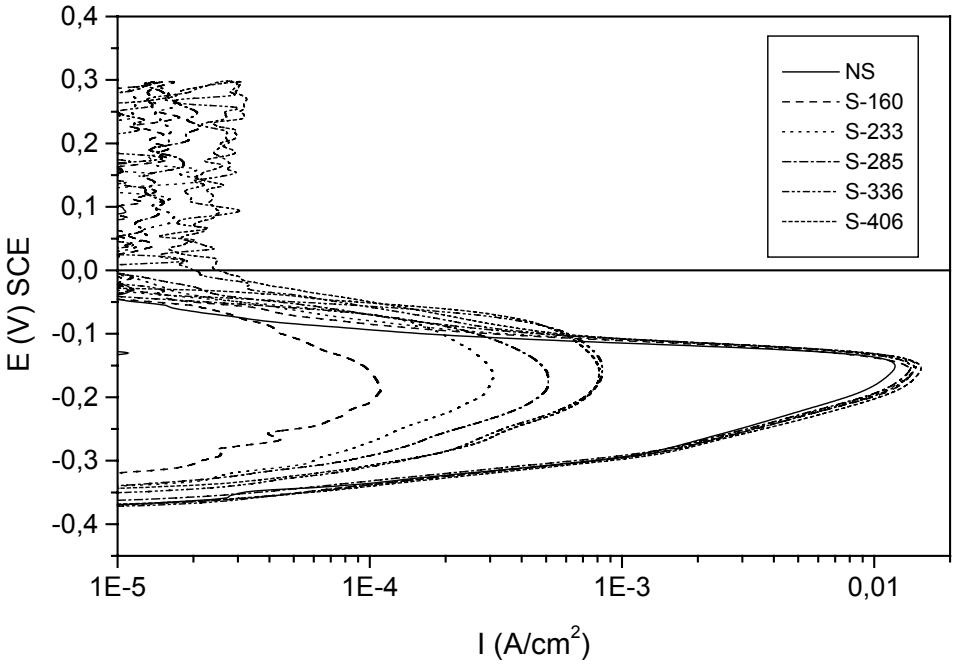

Figure IV-12. Polarization curves of specimens tested under experiment 12 conditions.

The final experiment in the list was given with code 12, which doesn't indicate any negative concern mentioned before and also it predicts the

results of the Streicher acid test with exceptionally good agreement and resolution. The polarization curves of specimens tested with parameters as given in the experiment 12, which are 1M H_2SO_4 + 0.005M KSCN and 3 V/hr scan rate, were given in Figure IV-12. As can be seen, there is a smooth transition as the state of the structure goes from step to dual and to ditch.

Finally to check the reproducibility of the test results, the S-233 (dual) and S-406 (ditch) specimens were tested successively ten more times under the conditions of the experiment 12. The mean, standard deviation, standard error and 95% confidence limits for potential, current and charge values were given in Table IV-13. It is found that, the passivation and depassivation potentials can be precisely obtained. Similarly the activation current and charge can be reproduced within a slight error margin. However for the reactivation currents and charges there is some variation, where its magnitude increases for the ditch structure. Nevertheless it is believed that, the results were reproduced within an acceptable error margin.

According to the proposed test parameters, one can then postulate that specimens giving I_r:I_a ratio higher than 4.0 can be classified as the ditch structure. The upper limit for the dual structure is therefore 4.0. The determination of lower limit for the dual structure, however is not evident. Comparing the weight loss acid test results, it was seen that the *ipm* of S-160 (dual) structure was found to be at most five times more than the *ipm* of S-51 (step) structure. Therefore, in order to set a value for the lower limit of the dual, we took the one fifth of the I_r:I_a value of the S-160 specimen which is 0.15. Therefore it is assumed that I_r:I_a giving values less than 0.15 classifies the step structure.

Table IV-13. Reproducibility of the DLEPR results for the S-233 and S-406 specimens with experiment 12 conditions. Statistical analysis was made over 11 samples.

		Mean	Standard Deviation	Standard Error	95% Confidence Range
S-233	Ea (V SCE)	-0.14644	0.00924	0.00279	-0.15264 : -0.14023
	Ia (mA/cm^2)	14.4460	0.4045	0.12120	14.1743: 14.7178
	Er (V SCE)	-0.17236	0.00713	0.00215	-0.17715 : -0.16756
	Ir (mA/cm^2)	0.3457	0.0625	0.01883	0.3038: 0.3877
	Qa (mC/cm^2)	1687.67	60.450	18.226	1647.06: 1728.28
	Qr (mC/cm^2)	63.599	11.928	3.596	55.586: 71.613
	Ir:Ia (x100)	2.388	0.396	0.1195	2.122: 2.654
	Qr:Qa (x100)	3.767	0.686	0.2068	3.306: 4.228
S-406	Ea (V SCE)	-0.15366	0.00656	0.00198	-0.15807 : -0.14925
	Ia (mA/cm^2)	16.0796	0.6746	0.20340	15.6264: 16.5328
	Er (V SCE)	-0.14237	0.02269	0.00684	-0.15761 : -0.12718
	Ir (mA/cm^2)	0.9148	0.2170	0.06544	0.7690: 1.0606
	Qa (mC/cm^2)	1874.29	69.169	20.855	1827.82: 1920.76
	Qr (mC/cm^2)	182.49	41.808	12.606	154.41: 210.58
	Ir:Ia (x100)	5.668	1.193	0.3597	4.867: 6.470
	Qr:Qa (x100)	9.711	2.038	0.6145	8.342: 11.080

Chapter V

CONCLUSIONS

In this study, the effect of scan rate, solution temperature and composition on the anodic polarization and the reactivation behavior of AISI 304L and 316L stainless steel was investigated, from which a criteria can be obtained for the determination of susceptibility to intergranular corrosion in these steels. This criteria, I_r:I_a or the Q_r:Q_a ratio, is the basis of the DLEPR method. The arbitrary choice of these test parameters might be misleading. Therefore in order to devise a procedure for the correct prediction of the degree of susceptibility to intergranular corrosion in these steels, DLEPR test parameters were systematically varied and correlated with the results of the weight loss acid tests and with the analysis of the microstructure, where finally, the following conclusions were drawn.

In the test solution, the presence of an activator is necessary, where KSCN fulfills this requirement quite effectively, whereas KCl was found not to be suitable, although, salts were used often for the reactivation of dual phase stainless steels. In this study, its effect was found not to be prominent and even sometimes detrimental because it is too aggressive especially for the AISI 304L type steel.

In general, I_r and I_a values increase similarly with the increase of H_2SO_4 content, thus constituting a weak functional dependence for the I_r:I_a ratio.

There is a weak dependence on scan rate for the activation behavior, but a strong influence for the reactivation. At high scan rates, during reactivation, time is not sufficient to breakdown the passive film, whereas there is plenty of time at low scan rates. Therefore for low scan rates I_r

increases, so does the I_r:I_a ratio. Therefore the improper choice of the scan rate can yield wrong results to be used for the prediction of susceptibility.

With the increased KSCN content in the test solution, there is an increase in anodic current but more complex behavior is seen on reactivation current. Nevertheless, I_r was always decreased for all specimen types when KSCN is at 0.02M concentration. Moreover, reactivation current profile changes with KSCN in such a way that it becomes skewed to higher potentials, where it is very obviously seen in the ditch structure. It is believed that this behavior is due to some surface activity taking place resembling the formation of metastable pits.

Current values increase with solution temperature because of the increase of chemical reactivity between solution and the passive film. It was understood that solution temperature should be kept constant to provide reproducibility and be controlled precisely.

DLEPR test presents quantitative results for 304L and 316L type steels. In the evaluation of sensitization in 316L type steel, in terms of I_r:I_a the best agreement with the weight loss acid tests were obtained with the following test parameters, 1M H_2SO_4 + 0.005M KSCN solution at 3 V/hr scan rate and with 30 °C solution temperature. Increasing the KSCN concentration, generally, still correlates well with the acid test results, but the resolution decreases slightly.

During corrosion reactions, it is the charge transfer that gives quantitative measures about the phenomena taking place. Therefore Q_r:Q_a criteria is expected to better represent the DLEPR result. However, since it was found to be very similar to I_r:I_a, and its computation requires sophisticated equipment, it is not found necessary to be used as the criteria of the DLEPR test.

The DLEPR test results can be reproduced with an acceptable error margin.

Finally, range of I_r:I_a for step, dual and ditch structures are determined to be 0 to 0.15, 0.15 to 4.0 and 4.0 and higher, respectively.

REFERENCES

1. ASTM A262-91: *Standard Practices for Detecting to Intergranular Attack in Austenitic Stainless Steel*.

2. ASTM G108-92: *Standard Test Method for Electrochemical Reactivation for Detecting Sensitization of AISI 304 and 304L Stainless Steel*.

3. Mason, J.F., *Corrosion Resistance of Stainless Steels in Aqueous Solutions*, in *Source Book of Stainless Steels*. American Society for Metals, Metals Park, OH, 1976.

4. Krivobok, V.N., *The Book of Stainless Steel*, in *American Society for Steel Treating*, E.E. Thum, Editor. Cleveland, OH, 1933.

5. Sahlaoui, H., K. Makhlouf, H. Sidhom, and J. Philibert, *Material Science and Engineering*, **A372** 98, (2004).

6. Shreir, L.L., *Corrosion.* George Newnes Ltd., London, 1963.

7. Sourmail, T., *Material Science and Technology*, **17** 1, (2001).

8. Pickering, F.B., *Physical Metallurgical Development of Stainless Steel* in Stainless Steel '84, 1985, G. L. Dunlop ed., Chalmers University of Technology, Göteborg, Institute of Metals.

9. Honeycombe, R. and H.K.D.H. Bhadeshia, *Steels Microstructure and Properties, 2nd ed.*, Edward Arnold, London, 1995.

10. Mulford, R.A., E.L. Hall, and C.L. Briant, *Corrosion-NACE*, **39** 132, (1983).

11. Bruemmer, S.M., *Corrosion*, **46** 698, (1990).

12. Hall, E.L. and C.L. Briant, *Metallurgical Transactions A*, **15A** 793, (1984).

13. Weiss, B. and R. Stickler, *Metallurgical Transactions*, **3** 851, (1972).

14. Lai, J.K.L., *Materials Science and Engineering*, **58** 195, (1983).

15. Minami, Y., H. Kimura, and Y. Ihara, *Materials Science and Technology*, **2** 795, (1986).

16. Schwind, M., J. Kallqvist, J.O. Nilsson, J. Agren, and H.O. Andren, *Acta Materialia*, **48** 2473, (2000).

17. Wallen, B. and J. Olsson, *Corrosion Resistance in Aqueous Media*, in *Handbook of Stainless Steel*, D. Peckner and I.M. Bernstein, Editors. McGraw-Hill, New York, 1977.

18. Beauchamp, R.L., Ph. D. Dissertation. Ohio State University, 1966.

19. Olefjord, I., B. Brox, and U. Jelvestam, *Journal of the Electrochemical Society*, **132** 2854, (1985).

20. Clayton, C.R. and I. Olefjord, *Passivity of Austenitic Stainless Steel*, in *Corrosion Mechanism in Theory and Practice*, P. Marcus and J. Oudar, Editors. Marcek Dekker Inc., New York, 1995.

21. Sedriks, A.J., *Metallurgical Aspects of Passivation of Stainless Steels* in Stainless Steel '84, 1985, G. L. Dunlop ed., Chalmers University of Technology, Göteborg, Institute of Metals.

22. Uhlig, H., *History of Passivity, Experiments and Theories*, in *Passivity of Metals*, R. Frankenthal and J. Kruger, Editors. The Electrocemical Society, Princeton, 1978.

23. Uhlig, H.H. and R.W. Revie, *Corrosion and Corrosion Control, 3rd ed.*, John Wiley and Sons Inc., New York, 1985.

24. Olsson, C.O.A. and D. Landolt, *Electrochimica Acta*, **48** 1093, (2003).

25. Strehblow, H.H., *Passivity of Metals*, in *Advances in Electrochemical Science and Engineering Vol.8*, R.C. Alkire ed., Wiley-VCH, 2002.

26. Olefjord, I. and B.O. Elfstrom, *Corrosion-NACE*, **38** 46, (1982).

27. Sugimoto, K. and Y. Sawada, *Corrosion Science*, **17** 425, (1977).

28. Tomashov, N.D. and G.P. Chernova, *Passivity and Protection of Metals against Corrosion.* Plenum Press, New York, 1967.

29. Jones, D.A., *Principles and Prevention of Corrosion, 2nd ed.*, Prentice Hall, N.J., 1996.

30. Delong, W.B., *ASTM STP*, **93** 211, (1949).

31. Alger, J.V., E.C. Roberts, R.P. Lent, and G.W. Anderton, *Bulletin of American Society for Testing and Materials*, **214** 57, (1956).

32. Truman, J.E., *Journal of Applied Chemistry*, **4** 273, (1954).

33. Marshall, H.B., *Corrosion-NACE*, **30** 1, (1974).

34. Sedriks, A.J., *Corrosion of Stainless Steels, 2nd ed.*, Wiley, New York, 1996.

35. Cihal, V. and R. Stefec, *Electrochimica Acta*, **46** 3867, (2001).

36. Clarke, W.L., W.M. Romero, and J.C. Danko, in Corrosion77, reprint no 180, National Assoc. of Corrosion Engineers, Houston, 1977.

37. Novak, P., R. Stefec, and F. Franz, *Corrosion*, **31** 344, (1975).

38. Desestret, A., P. Guiraldenq, and M. Froment, in 23rd Meeting of I.S.E., Stockholm, 1972.

39. Knyazheva, V.M., *Zashch. Metall.*, **4** 420, (1972).

40. Charbonier, J.C., *IRSID COS Report*, No: 74/58, 1974.

41. Umemura, F., M. Akashi, and T. Kawamoto, *Boshoku Gijutsu (Corr. Eng. Jpn.)*, **29** 163, (1980).

42. Umemura, F. and T. Kawamoto, *Boshoku Gijutsu (Corr. Eng. Jpn.)*, **28** 24, (1979).

43. Borella, A. and A. Mignone, *Br. Corros. J.*, **17** 176, (1982).

44. Majidi, A.P. and M.A. Streicher, *Corrosion*, **40** 584, (1984).

45. Cihal, V., *Corrosion Science*, **20** 737, (1980).

46. Majidi, A.P. and M.A. Streicher, *Corrosion-NACE*, **40** 393, (1984).

47. Jargelius, R.F.A., S. Hertzman, E. Symniotis, H. Hanninen, and P. Aaltonen, *Corrosion*, **47** 429, (1991).

48. Maday, M.F., A. Mignone, and M. Vittori, *Corrosion Science*, **28** 887, (1988).

49. Ahn, M.K., H.J. Kwan, and J.H. Lee, *Corrosion*, **51** 441, (1995).

50. Wu, T.F. and W.T. Tsai, *Corrosion Science*, **45** 267, (2003).

51. Wu, T.F., T.P. Cheng, and W.T. Tsai, *Journal of Nuclear Materials*, **295** 233, (2001).

52. Roelandt, A. and J. Vereecken, *Corrosion-NACE*, **42** (1986).

53. Zahumensky, P., S. Tuleja, J. Orszagova, and J. Janovec, *Corrosion Science*, **41** 1305, (1999).

54. Matula, M., L. Hyspecka, M. Suoboda, V. Vodarek, C. Daybert, J. Galland, Z. Stonawska, and L. Tuma, *Materials Characterization*, **46** 203, (2001).

55. Lopez, N., M. Cid, M. Puiggali, I. Azkarate, and A. Pelayo, *Materials Science and Engineering*, **A 229** 123, (1997).

56. Goodwin, S.J., B. Quayle, and F.W. Noble, *Corrosion-NACE*, **43** 743, (1987).

57. Fang, Z., Y.S. Wu, L. Zhang, and J.Q. Li, *Corrosion*, **54** 339, (1998).

58. Fang, Z., L. Zhang, Y.S. Wu, J.Q. Li, D.B. Sun, G. Jiang, and Z.M. Cui, *Corrosion*, **51** 125, (1995).

59. Huang, H., C.Liu, and S. Chen, *Corrosion*, **48** 509, (1992).

60. Liu, C., H. Huang, and S. Chen, *Corrosion*, **48** 686, (1992).

61. Cheng, X.L., H.Y. Ma, S.H. Chen, R. Yu, X. Chen, and Z.M. Yao, *Corrosion Science*, **41** 321, (1999).

62. Bühler, H.E., L. Gerlach, O. Greven, and W. Bleck, *Corrosion Science*, **45** 2325, (2003).

63. ASTM G5-87: *Standard Reference Test Method for Making Potentiostatic and Potentiodynamic Anodic Polarization Measurements*.